Dear editor

In the following you will find all our answers to the referee comments. The marked-up manuscript is attached at the end of this file.

We believe that the suggestions and comments of the Referees have substantially contributed to the improvement of the manuscript and we hope that it is acceptable for publication in *Atmospheric Measurement Techniques*.

Kind regards

Christine Aebi

Reply to comments by P. Kuhn (Referee #1)

on the manuscript "Cloud fraction determined by thermal infrared and visible all-sky cameras" by Aebi et al., submitted to Atmospheric Measurement Techniques.

We would like to thank the referee for the constructive comments that contributed to the improvement of the manuscript. Detailed answers to the comments are given below (bold: referee comment, regular font: author's response, italic: changes in the manuscript).

Summary
This script is concerned with an interesting and important field of research and should be published once major improvements are included.

Major comments:
1. **I somewhat feel that the title could be more concise: Maybe you could add the word "comparison" and state the names of the used cameras.**

We valued your suggestion, but we think that the title is adequate to the content of the paper. We would also prefer to have the title as concise as possible.

2. **Please discuss weaknesses / challenges of each studied system. How do the accuracies depend on (high) Linke turbidities, (low) solar angles or a "wet" atmosphere? What other situations could lead higher deviations? This could be an own section (for each system or combined). Please discuss this quantitatively, with plots and figures.**

Thanks for this comment. The authors are aware that at certain locations high turbidity situations, due to aerosols or water vapour, may lead to problems in analysing/interpreting the sky images. However, in Davos, throughout the year we measure rather low integrated water vapour (IWV) values (between 2 and 25 mm) and also low AOD values. Thus, for our study we cannot analyse the sensitivity of the cameras regarding these conditions.
Low solar angles can lead to a "whitening" of the images (as discussed in Long et al., 2006). Our Mobotix camera in Davos is installed on a solar tracker and the sun is shaded with a shading disk (as described on p. 8, l. 14f.). Therefore we do not have any problems with overexposed images due to low solar angles. Also with the Schreder camera we do not see any problems in situations with low solar angles.

3. **Please add another section or at least a distinct paragraph in the introduction focused on the discussion of satellite cloud products and ground-based cameras. There is a Himawari-8 satellite, apparently with a cloud product down to 250 m and a sampling rate down to 2.5 min. The competition for ground-based cameras may not be human observers, but such satellites (see also minor comment 7). Where do you see the application of your cameras? What advantages do you see in comparison to satellites? This discussion could include the silhouette effect and projection uncertainties relevant to ground-based point-like observers, but not present for satellites.**

We increased the length of the introduction and extended the paragraph discussing satellite measurements (p. 2, l. 6ff.):

An alternative to detect clouds from the ground by human observations is to detect them from space. With a temporal resolution of 5 to 15 minutes, Meteosat Second Generation (MSG) geostationary satellites are able to detect cloud coverage with a higher time resolution than is accomplished by human observers (Ricciardelli et al., 2010; Werkmeister et al., 2015). The geostationary satellite Himawari-8 (Da, 2015) even delivers cloud information with a temporal resolution of 2.5 to 10 minutes and a spacial resolution of 0.5 to 2 km. However, these geostationary satellites cover only a certain region of the globe. Circumpolar satellites (i.e. the MODIS satellites Terra and Aqua (Baum B.A., 2006; Ackerman et al., 2008)) determine cloud fraction globally, but for a specific region only four times a day. Satellites cover a larger area than ground-based instruments and are also able to deliver cloud information from regions where few ground-based instruments are available (e.g. in Arctic regions (Heymsfield et al., 2017) or over oceans). However, due to the large field of view (FOV) of satellites, small clouds can be overlooked (Ricciardelli et al., 2010). Another challenge with satellite data is the ability to distinguish thin clouds from land (Dybbroe et al., 2005; Ackerman et al., 2008). Furthermore, satellites collect information mainly from the highest cloud layer rather than the lower cloud layer closer to the earth's surface. Nowadays satellite data are validated and thus supported by ground-based cloud data. Different studies focusing on the comparison of the determined cloud fraction from ground and from space were presented by e.g. Fontana et al. (2013); Wacker et al. (2015); Calbo et al. (2016); Kotarba (2017).

However, at this point we would like to mention, that the paper focuses on the description of a new ground-based instrument that might serve as an alternative to human cloud observations (as mentioned on p. 3, l. 33ff.) and does not focus on cloud observations from satellites.

The authors added some more possible applications for the newly developed IRCCAM (p. 3, l. 35/p. 4, l. 1.):

Thus the IRCCAM could be used for different applications at meteorological stations, at airports or at solar power plants.

4. The challenges being present regarding human cloud observation are partially addressed. However, you might be able to enhance the discussion. What is "not objective" (p1, line 24)? What are the differences if several experts evaluate images? You might be able to find such figures, which would significantly increase the quality of this argument. There is a reference missing on p2, line 1, for "nighttime determinations are difficult" - again, if you could find a reference, this would be an improvement.

We extended and changed the paragraph about human cloud observations (p. 1, l. 20ff.):

The most common practice worldwide to determine cloud coverage, cloud base height (CBH) and cloud type from the ground are human observations (CIMO, 2014). These long-term series of cloud data allow climate studies to be conducted (e.g. Chernokulsky et al., 2017). Cloud detection by human observers is carried out several times per day over a long time period without the risk of a larger data gap due to a technical failure of an instrument. However, even with a reference standard defined by the World Meteorological Organisation (WMO) for human observers, the cloud determination is not objective e.g. mainly due to varying degrees of

experience (Boers et al., 2010). Other disadvantages of human cloud observations are that the temporal resolution is coarse and due to visibility issues nighttime determinations are difficult. Since clouds are highly variable in space and time, measurements at high spatial and temporal resolution with small uncertainties are needed (WMO, 2012). Recent research has therefore been conducted to find an automated cloud detection instrument (or a combination of such) to replace human observers (Boers et al., 2010; Tapakis and Charalambides, 2013; Huertas-Tato et al., 2017; Smith et al., 2017).

5. Similar to major comment 3: If you state that "thin clouds cannot be distinguished from land" (p2, l9), you might as well enter into a full scale discussion of the weaknesses of satellites (beneficial to the quality of this paper). Please clarify the statement. Similar: "collect mainly from the highest cloud levels" (p2, l11) – Can't satellites, to some extent, differentiate? What are these limitations / what is the advantage of ground-based cameras? Same argument hold for the next sentence: "in order to retrieve. . ." – these statements are very absolute. How good are the cloud products of satellites, having multiple channels / sensors? To my knowledge, thin ice clouds can be differentiated from cumulus clouds quite well.

As already mentioned in the answer to major comment 3, we extended the discussion about satellite cloud detection (p. 2, l. 6ff.). However, the authors would like to mention here again, that the main focus of the paper is on ground-based cloud detection and not on the cloud detection from satellites. Therefore, the authors think that it is not needed to go into further details about satellite experiments.

6. Maybe, there are more ways to determine cloud coverages, which were not mentioned in the introduction. For instance, cloud coverages could be estimated from PV-data or using downward-facing cameras (https://doi.org/10.1016/j.solener.2017.05.074, **https://doi.org/10.5194/asr-15-11-2018**).

Thanks for this comment, we included some more references in the text (for example p. 3, l. 13f.).

7. Please provide a cost estimate of all used systems.

From the used camera systems the one from Mobotix is the least expensive. The price of the Schreder all-sky camera is in the order of five times as much as the Mobotix camera and the IRCCAM in the order of fifty times a Mobotix camera.

8. P2, l. 28f: I'm not an expert on this, but radars (e.g. those rain radars in airplanes) have a "lack of information about the whole sky"?

The authors refer to cloud radar systems as for example described in Boers et al., 2010, which have a beam width of 0.3 degrees. Thus the cloud radars do also belong to the column cloud detection instruments.

9. P2, l. 30: Please clarify how a point-like measurement system such as a ceilometer can "detect", "with considerable accuracy", "a fully covered or cloud-free" situation. Isn't this just an assumption that the small measured cone is representative of the whole sky? Stationary clouds outside this cone would not be detected by the ceilometer.

We revised our sentence (p. 3, l. 6f.):

Boers et al. (2010) showed that with smaller integration times the instruments tend to give okta values of zero and eight rather than the intermediate cloud fractions of 1 to 7 oktas.

10. P2, l. 33: "The most common all-sky cameras are the total sky imager" – could you provide some figures on that? How many systems has Reuniwatt (or other companies) sold? Given the known issues with the TSI, one of which is its age, this might not be a very good reference.

We are aware that the TSI is an older (and even one of the pioneering instruments), but it is still one of the most common all-sky cameras (as also mentioned by the other two referees).

11. Update your references. You quote many old papers in an area of active research.

We added some more recent publications in the text (for example p. 2, l. 5).

12. P. 3, l. 3: "low cost commercial cameras" "give no information during nighttime. There are several commercially available IR surveillance cameras out there. Are you sure that they are not used in meteorology as of today?

It is possible that some other commercially available IR surveillance cameras than the ones mentioned in the text are used in meteorology. However, at present we do not have any knowledge or did not find any publication about them.

13. P. 3, l. 7ff: I think there are more IR systems, e.g. the Reuniwatt one. Maybe you can highlight the differences a bit more and improve the presentation (it is hard to get all the ranges out of the text).

Thanks for this comment. As it seems the Sky Insight thermal infrared cloud imager from Reuniwatt is very new on the market and we were not aware of this instrument before submitting our discussion paper. In the revised version we added a few sentences about this camera system (p. 3, l. 26ff.):

Relatively new on the market is the Sky Insight thermal infrared cloud imager from Reuniwatt. The Sky Insight cloud imager is sensitive in the 8 µm - 13 µm wavelength range and its layout and software is similar to the prototype instrument presented here.

To our knowledge, there is no publication about the performance of this instrument available yet. Therefore we cannot highlight any differences in the performance.

We also added another recent publication about an infrared sky imaging system (p. 3, l. 25f.):

Redman et al. (2018) presented a reflective all-sky imaging system (sensitive in the 8 µm - 14 µm wavelength range) consisting of a longwave infrared microbolometer camera and a reflective sphere (110° FOV).

14. Introduction: Please generally improve the readability and the structure of the introduction. Maybe sub-titles might help.

The introduction was extended and rewritten following most of the referee's remarks.

15. End of introduction: Clearly state your motivation to develop a new system? What are the advantages in comparison to other developments?

We further motivated the development of a new camera system (p.3., l. 33ff.):

The IRCCAM was developed to provide instantaneous hemispheric cloud coverage information from the ground with a high temporal resolution in a more objective way than human cloud observations. Thus the IRCCAM could be used for different applications at meteorological stations, at airports or at solar power plants.

16. P4, l. 22: Is there any reason why you assume a flat response curve? For cameras in the visible spectrum, the curve is very far from being flat. Isn't there a data sheet available?

We actually did not assume a flat response function and considered the response function we received from the manufacturing company. We included Figure 2, which shows the actual response function R_λ. We changed Equation 2 correspondingly as well as the description in the text. The conclusions of our study does not change regardless of the definition of the response function.

17. P5, l.1: I think I've just missed it: What does this calibration function include? Both the mirror deviations and potential deviations of the imaging system of the camera?

The camera was placed in front of a blackbody aperture for retrieving the calibration function. This function is then independent from the mirror. The function's purpose is to convert the output of the camera (i.e. the number per pixel) to brightness temperature and radiance respectively.

18. P5, l. 9: To my experience, calibrations (with cameras in the visible spectrum) conducted with the sun show relatively large deviations (as the sun disk is usually quite large). This is less of an issue for IR cameras. However, I wonder: Why did you choose the sun instead of the full moon or stars? Could you estimate the deviations (presumably very relevant for the algorithms in the circumsolar area) for this EOR?

The solar disk on the image covers an area of around 1°. Thus we think that the sun covers a very well defined area on the images and we do not see any problem to use the sun to remove the distortion of the images. The full moon is only visible during cloud-free conditions and thus not practical to use it as a reference to undistort the images. Stars are not visible at all on the images.

19. Figure 3 c: Please provide a scatter density plot over all days similar to this figure. There seems to be an offset in the center, which might be better visible or disappear if more data are studied.

We are aware that there is an offset in the center of the images. Our analysis on p. 6, l. 28ff. is showing that there is an average difference between the measurement and the model of 4 K ±2.4 K which stems to a certain degree from this offset in the center. However, the authors think that this offset is not relevant for the present study to determine the cloud fraction.

20. P6, l. 1: I was wondering about the mirror temperature and potential asymmetries. Could you briefly state if the one-sided heating of the sun leads to a temperature distribution on that mirror within your stated 1 K range? In Fig. 1, a wall is visible close to the IR-camera – is there a problem with radiated heat, e.g. during night-times? Could you briefly state something on the interplay between the ground temperature and that mirror? Do you expect aging effects on the mirror? How bad is the soling?

We did not see any problems with asymmetries in the temperature distribution on the mirror. We also did not see any effect of the wall next to the IRCCAM on the sky brightness distribution on the mirror. However, what we have seen is the larger longwave emissivity from Davos (SSW direction), which leads to a false classification of cloudy pixels on the images in direction of Davos. This problem is briefly discussed on p. 10, l. 4ff.:

It is noteworthy that the IRCCAM clearly underestimates the occurrence of 0 oktas in comparison to the cameras measuring in the visible spectrum (by up to 13 %). On the other hand, the relative frequency of the IRCCAM of 1 okta is clearly larger (by up to 10 %) compared to the visible cameras. This can be explained by higher brightness temperatures measured in the vicinity of the horizon above Davos. These higher measured brightness temperatures are falsely determined as cloudy pixels (up to 0.16 cloud fraction). Since these situations with larger brightness temperatures occur quite frequently, the IRCCAM algorithm detects more often cloud coverages of 1 okta instead of 0 okta.

So far the mirror did not show any relevant aging issues.

21. P6, l 7f: You are stating absolute values here, saying that there are no differences between night and day data. Does this also hold for relative figures (I assume that the temperatures at night are lower)?

The absolute differences between night and day are 4.32 K ±2.3 K and 3.86 K ±2.5 K respectively. In relative numbers, the difference between day and night is around 0.2 % and thus negligible.

22. P6, l. 18: I somewhat doubt if the "observed discrepancy of 4 K" is only caused by model parameters (which one? Your LUT?). Please make this discussion a bit more wholesome. Other attributing factors might be camera instabilities and maybe the effects named in major comment 20.

We changed the sentence (p. 7, l. 1ff.):

Therefore, the observed discrepancy of 4 K between measurements and model calculations mentioned previously can probably be attributed to the uncertainties in the model parameters (temperature and IWV) used to produce the LUT.

23. P6, l. 29: Please further motivate the threshold of 6.5 K. This might be done with an example image, including clouds. Was this threshold somewhat fitted to the data?

The threshold of 6.5 K is empirically defined. We chose this rather large threshold to minimise the probability that cloud-free pixels are (wrongly) classified as clouds (described on p. 7, l. 16ff.). The second part of the algorithm decides whether thin (and therefore low-emissivity) clouds) are present or not.

24. Section 2.1.1 – please enhance visualization, e.g. using a flow-chart or pseudocode.

We slightly changed the description of the algorithm and are convinced that the changes increased the readability of this section.

25. P7, l. 4: I'm wondering how big intra-cloud temperature variations are. Could it be that parts of the cloud are detected as such while some pixels within are below the thresholds? If so, algorithms such as region growing or compression based approaches might enhance the segmentation.

What we see from the images is that there is a smooth decrease of the brightness temperature at the border of the clouds. Thus it becomes more difficult to detect certain pixels as clouds the smaller the difference in brightness temperature to cloud-free pixels is. This behaviour makes it also difficult to detect thin (low emissivity) clouds. In order to possibly improve the determination of thin cirrus clouds, a pattern recognition algorithm could be tested in a further study.

26. P7, l. 6: If possible, further motivate the threshold of 1.2 K – is there a physical explanation?

The threshold of 1.2 K is empirically defined. Different thresholds were tested for a certain number of images and thereafter we chose the threshold of 1.2 K because it was the best fit between classifying and mis-classifying cloudy/non-cloudy pixels.

27. P7, l. 11: Quantify "usually". Elaborate on the whole paragraph (this corresponds to a general discussion of challenging situations and weaknesses of this device and does not have to be done at this position. I suggest dedicating a whole section to this discussion).

We removed these sentences from this section.

28. P7, l. 30: Why did you choose a custom resolution for the Mobotix camera? To my experience, 1/500 is a very bright exposure time (this might be solved by blocking out the sun, but I'm curious) – is this an issue? You are using ratios to segment clouds, why did you not use an automatic exposure time?

Our Mobotix camera is installed on a solar tracker and is shaded with a shading disk (as mentioned on p. 8, l. 14f.) and the bright exposure time is therefore not an issue.

29. P8, l. 4: Please provide a brief statement on how good the Mobotix system performs under high turbidity conditions, using a simple threshold-based approach, as well as for low solar elevations.

See the answer to major comment 2.

30. Specify the total run time of each algorithm.

To calculate the cloud fraction from the two visible cameras for a full day takes on a personal computer a few minutes whereas the calculation of the cloud fraction from the IRCCAM takes 30-60 minutes.

31. P8, l 19: 70° - isn't it quite a problem if the FOV of all systems is not the same? Cloud coverages might be correctly detected but yet different. The same holds for different occlusions.

Indeed it is a problem if the FOV of all systems is not equal. This problem is also briefly discussed in different paragraphs of the paper (e.g. p. 11, l. 9ff.).

32. Specify the distance between the cameras, provide example images for all.

The distance between the Mobotix and the Schreder camera is roughly six meters. The IRCCAM is roughly 70 m and 76 m away from the Schreder and the Mobotix camera respectively.

33. Section 3.2: Aggregating the figures to 1/8-bins clearly reduces the deviations between the systems. This is good for many applications in nowadays meteorology. However, I wonder how much the deviations increase if the images are compared pixelwise. Could you provide these figures?

Thanks for this comment. It would be indeed interesting to compare the different cameras pixelwise, however, for the aim of our study, presenting a new camera system to detect clouds for synoptic purposes, this analysis is out of scope.

34. Section 3.2.3: Please motivate why you assumed seasonal differences – what are the origins of the deviations? It is presumably not earth's inclination towards the sun. Identify these parameters and study them separately. Example: I could imagine that e.g. a wet atmosphere poses challenges for the IR system. A wet atmosphere can happen both during winter and during summer times (with different probabilities). Aggregating over many different conditions might make analyses more difficult.

We added a motivation for the seasonal analysis (p. 13, l. 17ff.):

The seasonal analysis is performed in order to investigate whether a slightly unequal distribution of cloud types in different months in Davos (Aebi et al., 2017) have an impact on the performance of the cloud fraction retrieval between seasons.

35. You could separate a new section "Next steps" (or similar) from the conclusion, stating in more detail what could be made to further improve the system and why you think this would lead to more accurate results.

On p. 14, l. 26ff. we mentioned different points that could be tested in order to improve the system:

However, the known brightness temperature distribution of the sky and thus the known radiance can also be used for other applications including the determination of other cloud parameters (cloud type, cloud level, cloud optical thickness) as well as the retrieval of information about downward longwave radiation in general. Thus, after some improvements in the hardware (e.g. a heating or ventilation system to avoid a frozen mirror) and software (improvements of the cloud algorithm detecting low-emissivity clouds by e.g. pattern recognition) the IRCCAM might be of interest for a number of further applications for example at meteorological stations or airports.

36. Figure 5.: There is an interesting offset visible at around 7.00 (please state timezone, UTC+0?) – how comes? Is this caused by a different FOV or different occlusion affecting the systems?

Thanks for this comment. There were two time steps that had an extremely large cloud fraction determined by the IRCCAM. During those two time steps someone was cleaning the mirror with distilled water. A mirror covered with water leads to high emissivity values which are wrongly detected as clouds. Therefore we removed now these two data points from the Figure (now Figure 6).

37. Figure 6.: Please add a colorbar for Fig. 6b. Did you bother to mask out the camera arm and the suspension? The forest to the right is very finely masked out – couldn't there be minor issues due to moving trees?

We added the temperature range to the caption of the Figure. The features depicted on Figure 7c (before Figure 6c) are the shading disks of three sun trackers. Thus they are moving and therefore it is difficult to mask them out without losing information about the sky pixels. In Figure 7c (before Figure 6c), these shading disk covers an area of only 0.4 %. The area between the trees covers less than 0.01 % of the analysed pixels and is therefore not relevant for the current study, even in cases of moving trees.

38. Figure 7.: I might have missed it, but is there so far a discussion on this bias included in the script? (also Fig. 9). Could you provide the same plots for a Mobotix-Schreder comparison? This would help to evaluate the references.

The focus of our study is to present and validate the performance of the IRCCAM regarding cloud fraction determination. Therefore, the authors are convinced that it is not relevant to increase the discussion about the comparison between Mobotix and Schreder cameras.

39. In general: You compare cloud fraction estimations from different systems, all of which are not completely accepted by everyone in the community. Potentially, it could further strengthen your line of argumentation if you included a comparison against a more established approach. This could be (1) satellites or (2) a comparison to a clear sky index derived from DNI measurements over the whole period (3), also unrealistic, from PV data or (4) from ceilometer data. Presumably, (2) is the way to do it.

The Mobotix camera has been validated against and compared with data from satellites, human observers and a ceilometer in former studies (for example in Wacker et al., 2015). Those studies are a valid argument for using the Mobotix camera as a reference for the validation of the newly

developed IRCCAM. In Davos we do not have possibilities to compare our data with ceilometer or PV data. As mentioned in the paper as well as in several answers here, the study focuses on the cloud detection with ground-based instruments and not on comparisons with satellite data.

40. Table 5.: 1 okta is quite a lot and I'm a bit concerned about the rather low values visible here (e.g. 59%). Maybe, looking at pixel-wise deviations (major comment 33) could cast a light on the origins of these rather large deviations. This is clearly as good as or even better than human observers, but I think satellite cloud products and other camera systems (e.g. https://doi.org/10.1002/pip.2968 or the works from Stefan Winkler) achieve smaller deviations.

The focus of the paper is to present a newly developed ground based camera that might be used for example at meteorological stations, airports or solar power plants. At meteorological stations the state of the art unit for cloud fraction is oktas (also defined by WMO).
As we already mentioned in the major comment 3 and 5, the focus of the paper is on ground-based measurements and not on satellite data.

41. Table 6.: You state that there are no significant deviations between the seasons. This is only partially backed by the figures in this table. Please clarify in greater detail.

We extended the discussion in Section 3.2.3 (p. 13, l. 25ff.):

The slight difference between the two seasons might be explained by the slightly larger frequency of occurrence of the thin and low-emissivity cloud class cirrocumulus-altocumulus in Davos in summer than in winter (Aebi et al., 2017).

Minor comments:

1. I'm just wondering: Is there no English name for "Physikalisch-Meteorologisches Observatorium Davos/..."?

This is the official affiliation of our institute and is therefore not translated.

2. In general, the language used could be a bit more fluent. Examples are "other study instruments" in the abstract ("other instruments used here") or "coverage of the sun with clouds" (p1, line 18).

Done

3. A short summary of major comment no 2 (challenges) should find its way into the abstract.

See the answer to major comment number 2.

4. I might have missed it, but why are there, in the abstract, two figures for low-level cloud, and one figure each for mid-level and high-level clouds?

The abstract has been rewritten to a larger part.

5. Please rephrase the sentence between p1, line 17 and p1, line 19 (subpar English).

Done

6. P1, line 20, the position of "globally" seems to be odd. I furthermore disagree with that statement - there are more cloud observations made by satellites than by human observers.

Following most of your recommendations, we changed a large fraction of the introduction.

7. P1, line 21: Human observation has the "advantage" to be carried out "several times per day" - satellites have a higher sampling rate, what you also mention later.

Following most of your recommendations, we changed a large fraction of the introduction.

8. P1, line 23: "there is no reference standard for human observers" - really? No manual from any organization?

We rewrote the sentence on p. 1, l. 23ff.:

However, even with a reference standard defined by the World Meteorological Organisation (WMO) for human observers, the cloud determination is not objective e.g. mainly due to varying degrees of experience (Boers et al., 2010).

9. P1, line 23: Humans are "independent of any technical failure" - please rephrase.

Done

10. P2, l. 2, leave out "measurement"

Done

11. P2, l. 2, This sentence could be rephrased to something like "Recent research has therefore been conducted to find automated cloud detection instruments to ..." (more concise English). You might mention the DWD objective to automate its stations in the next years.

Following most of your recommendations, we changed a large fraction of the introduction.

12. P2, l.5, is "synoptic" the correct word here? What do you want to say?

Following most of your recommendations, we changed a large fraction of the introduction.

13. P2, l. 5. "time resolution of 15 min", there is a rapid scan method with 5 min

We changed the sentence on p. 2, l. 6ff.:

With a temporal resolution of 5 to 15 minutes, Meteosat Second Generation (MSG) geostationary satellites are able to detect cloud coverage with a higher time resolution than it is accomplished by human observers (Ricciardelli et al., 2010; Werkmeister et al., 2015).

14. P2, l. 11, "Earth" could be written "earth".

Done

15. P2, l. 13, you measure the cloud coverage, not the cloud in general, "cloud measurement techniques".

Done

16. P.2, l. 14: maybe "certain" instead of "different" (from what?). Also "radiometers" – do you mean scanning radiometers? For the clear-sky algorithms based on GHI and DHI measurements?

We changed the whole paragraph.

17. P2, l. 25: You use "reflected" and "scattered" in a very similar way. Maybe "backscattered" is better suited?

Done

18. P3, l. 3: maybe "development" instead of "deployment"?

Done

19. P3, l. 16: state also here which "commercial thermal camera" you use.

Done

20. You might clarify the term FOV. Once it is used for the camera and once for the whole system. Is it really 180°?

The IRCCAM has a field of view of 180°. But the effective view of the sky is defined by the horizon, which is in a mountainous area as Davos clearly less than the 180°.

21. P3, l. 27. Please clearly state also here the models of the used cameras.

Done

22. P3, l. 28: "and a newly developed" -> "and the newly developed"

Done

23. P4, l. 9, rephrase, there are too many "and"s

Done

24. P4, l. 9, high -> large / tall

Done

25. P5, l. 25f: Rephrase/shorten the sentence. You might try to shorten other sentences as well.

Done

26. General: I think this is not your fault, but I'd prefer having the images directly in the text, not at the end of the script.

This is indeed not the decision of the authors, but the guideline of the journal.

Reply to comments by J. Calbó (Referee #2)

on the manuscript "Cloud fraction determined by thermal infrared and visible all-sky cameras" by Aebi et al., submitted to Atmospheric Measurement Techniques.

We would like to thank the referee for the constructive comments that contributed to the improvement of the manuscript. Detailed answers to the comments are given below (bold: referee comment, regular font: author's response, italic: changes in the manuscript).

This paper introduces a new sky camera, specifically an infrared camera which can take sky images both in daylight and nighttime conditions. The paper explains the algorithm that is applied to derive cloud cover from the images of this camera. Moreover, a thorough validation-comparison effort is performed between cloud cover derived from these images, from images of other two (visible, that is, only during daylight hours) commercial sky cameras, and from the APCADA algorithm (based on cloud effect on downward longwave radiation measured with a pyrgeometer).
In some way this paper is a follow-on of a previous paper by the same research group (Aebi et al, 2017, AMT) where they presented an analysis of a long series of diurnal cloud cover obtained with a sky camera. The present paper, however, has several added values: the introduction of a new concept of an infrared sky camera (looking downwards to a convex mirror), the suggestion of the method for image processing, and the comparison with other estimations of cloud cover. Therefore, the paper is worth of being published in AMT. It seems to me that a few changes could be considered to make it more complete and to get higher impact in the scientific community, but even in the present version, the paper may be good enough to merit publication.

Suggested general change:

1. In order to make more significant the comparison among all estimations of cloud cover, authors could consider applying exactly the same horizon mask to all images. For example, they could use a mask for the part of the image that is below 70 deg. SZA (20 deg. over the "flat" horizon). In fact, even APCADA algorithm is unsensitive to clouds that are in the horizon, so using this mask for all images would make the comparison more homogeneous.

Thanks for this comment. The authors are aware that the comparison of the cameras and APCADA are problematic when different horizon masks and different field of views are considered. However, the focus of the paper is mainly to present a new camera system (IRCCAM) and to show the possibilities of this new camera system. Thus we decided to not decrease the field of view of the IRCCAM due to the fact that one of the camera software is not able to detect clouds below 70°.

Minor changes and technical details to be corrected:

2. The word "significant" is used several times in the manuscript. I have my doubts about this use, as no statistical tests are applied (at least, they are not mentioned). So I would suggest use "significant" with caution, as it has a meaning related to statistical tests. If possible, try to use another word. In page 11, line 25, it is said that a difference of 0.02 is statistically not significant, but with no reference to what statistical test is applied.

We exchanged the word significant throughout the manuscript.

3. In lines 13-24 tow different approaches for cloudiness estimation are summarized. But in my opinion they are not clearly differentiated. Calbó et al 2001 suggests a method based on pyranometer measurements (i.e., hemispheric measurement of solar irrandiance), which is very different to Nephelo or Nubiscope, which are measuring in the infrared and in a narrow field of view. Please consider slightly modifying the writing of this paragraph.

We changed the writing of this paragraph (p. 2, l. 20ff.):

…. Depending on the wavelength range, the presence of clouds alters the radiation measured at ground level (e.g. Calbo et al., 2001; Mateos Villàn et al., 2010). Calbo et al. (2001) and Dürr and Philipona (2004) both present different methodologies to determine cloud conditions from broadband radiometers. Other groups describe methodologies using instruments with a smaller spectral range. Such instruments are for example the infrared pyrometer CIR-7 (Nephelo) (Tapakis and Charalambides, 2013) or Nubiscope (Boers et al., 2010; Feister et al., 2010; Brede et al., 2017), ….

4. I wouldn't say that WSI is among the most common all-sky cameras (as it is indeed the TSI). The WSI is one of the pioneering cameras, and presents very interesting characteristics and developments, but, to my knowledge, is no usually commercialized and therefore, is not quite common.

We changed the sentences discussing the TSI and the WSI (p. 3, l. 8f.):

The most common all-sky camera is the commercially available total sky imager (TSI) (Long et al., 2006). Another pioneering hemispherical cloud detection instrument is the whole sky imager (WSI) (Shields et al., 2013).

5. Eq (3). Could you explain why the zenith angle is divided by 65?

Equation 3 is a normalized function to fit the sky brightness temperature. Since we are taking the sky brightness temperature at 65° (T_{65}), we also divide by 65. Smith and Toumi, 2008 present the example to normalize at 90°, but in our case 90° is not representing the sky, but the mountains.

6. It is interesting to note that different thresholds are used in the processing of the visible images. This could partly explain some of the difference found in this paper. In fact, selection of the threshold is critical to distinguish between a cloudy pixel, and a clear (but sometimes, containing aerosol) pixel. Some discussion on this matter may be found in Calbó et al 2017 (and other studies cited therein). [Calbó, J., C. N. Long, J. González, J. Augustine, and A. Mccomiskey, 2017: The thin border between cloud and aerosol: Sensitivity of several ground based observation techniques. Atmos. Res., 196, 248–260, doi:10.1016/j.atmosres.2017.06.010.]

We added the reference in the conclusion (p. 14, l. 10ff.):

Differences in the cloud fraction estimates can be due to different thresholds for the camera systems (as discussed in Calbo et al. (2017)) as well as some other issues addressed throughout the current study.

7. The authors recognize that IRCCAM fails at both extremes of the cloud cover distribution. This (unexpected) result should merit more attention, with a deeper discussion if possible.

We added a short discussion about a possible reason for this distribution (p. 10, l. 4ff.):

It is noteworthy that the IRCCAM clearly underestimates the occurrence of 0 oktas in comparison to the cameras measuring in the visible spectrum (by up to 13 %). On the other hand, the relative frequency of the IRCCAM of 1 okta is clearly larger (by up to 10 %) compared to the visible cameras. This can be explained by higher brightness temperatures measured in the vicinity of the horizon above Davos. These higher measured brightness temperatures are falsely determined as cloudy pixels (up to 0.16 cloud fraction). Since these situations with larger brightness temperatures occur quite frequently, the IRCCAM algorithm detects more often cloud coverages of 1 okta instead of 0 okta.

8. The first lines of section 3.2.3 (lines 21-29) do not address seasonal analyses, so I suggest moving them to another section.

We moved these lines to section 3.2.

9. Somewhere in the Results or Conclusion sections, I would appreciate a short discussion of the present results in comparison with performance of other IR whole sky cameras (if you can find any) or other sky cameras that take night images. If no previous work can be found with an estimation of the performance of such night images, this should be highlighted in the paper. Suggested references: [Shields, J. E., M. E. Karr, R. W. Johnson, and A. R. Burden, 2013: Day/night whole sky imagers for 24-h cloud and sky assessment: history and overview. Appl. Opt., 52, 1605–1616, doi:10.1364/AO.52.001605; Gacal, G.F.B. Antioquia, C., and N. Lagrosas, 2016: Ground-based detection of nighttime clouds using a digital camera. Appl. Opt., 55, 6040–6045, doi:10.1364/AO.55.006040.]

The authors could not find any comparisons to other IR whole sky camera systems.

10. Figure 4, caption and related text. There is some mistake in the definition of oktas from cloud fraction. According with the caption, 0 oktas is for cloud fraction between 0 and 0.05 (which looks correct to me) but 8 oktas is between 0.875 and 1.0, that is a much larger interval, which seems wrong (at least, it is not symmetrical). And, for example, 4 oktas should be 0.4375-0.5625 (that is, a bin centered in 0.5 with a width of 0.125). If you correct this, some differences among the methods may change.

Thanks for this comment. The description of the okta ranges in the caption of Figure 5 (before Figure 4) was indeed wrong and we corrected it. However, the analysis was done with the correct ranges.

11. Table 1 and table 2 could be put together in a single matrix-like table (like the authors do in Table 5). In each cell (only in one triangle of the matrix) both the median and the percentiles may be written (for example, as 0.01 [-0.24,0.21].

Since Table 1 and Table 2 are placed in the corresponding sections where they are discussed, we decided to not merge them.

Reply to comments by Anonymous Referee #3

on the manuscript "Cloud fraction determined by thermal infrared and visible all-sky cameras" by Aebi et al., submitted to Atmospheric Measurement Techniques.

We would like to thank the referee for the constructive comments that contributed to the improvement of the manuscript. Detailed answers to the comments are given below (bold: referee comment, regular font: author's response, italic: changes in the manuscript).

This manuscript introduces a new infrared sky camera and an applied cloud detection algorithm and a comparison with visible sky cameras. It represents a substantial contribution to scientific progress within the scope of AMT. The image processing method, based on down-welling longwave radiation, to estimate the amount of cloud cover is a unique approach, as is the determination of cloud type. I recommend that the manuscript be published, with consideration of the following comments.

1. **Page 2, Line 33: The TSI is indeed probably the most common all-sky camera but the Solmirus ASIVA or Reuniwatt Sky InSight may currently be more common than the WSI.**

Thanks for this comment. We included a short description about the Reuinwatt Sky InSight cloud imager in our introduction (p. 3, l. 26ff.):

Relatively new on the market is the Sky Insight thermal infrared cloud imager from Reuniwatt. The Sky Insight cloud imager is sensitive in the 8 μm - 13 μm wavelength range and its layout and software is similar to the prototype instrument presented here.

We also slightly adapted the paragraphs discussing the TSI, WSI and the Solmirus ASIVA:

p. 3, l. 8f.:
The most common all-sky camera is the commercially available total sky imager (TSI) (Long et al., 2006). Another pioneering hemispherical cloud detection instrument is the whole sky imager (WSI) (Shields et al., 2013).

p. 3, l. 19ff.:
Another instrument, the Solmirus all-sky infrared visible analyser (ASIVA) consists of two cameras, one measuring in the visible and the other one in the 8 μm - 13 μm wavelength range (Klebe et al., 2014).

2. **Page 6, Line 23: A better description is needed for "IRCCAM frame". Does this include the camera, arm, and wire ropes?**

Yes, the term "IRCCAM frame" includes the camera, arm and wire ropes. We clarified this in the text (p. 7, l. 7ff.):

This image mask contains local obstructions such as the IRCCAM frame (camera, arm and wire ropes) as well as the horizon, which in the case of Davos consists of mountains limiting the field of view of the IRCCAM.

3. 3. Page 6, Line 20, Page 8, Line 2, and Page 8, Line 20: The horizon mask appears to be independently defined for each image and for each of the three cameras. Using the same horizon mask for all images would yield a better comparison.

There is only one horizon mask per camera (we clarified this now in the text). Because the resolution and the location of the three cameras is slightly different, we decided to define one horizon mask per camera system and not using the same for all systems.

Cloud fraction determined by thermal infrared and visible all-sky cameras

Christine Aebi[1,2], Julian Gröbner[1], and Niklaus Kämpfer[2]

[1]Physikalisch-Meteorologisches Observatorium Davos, World Radiation Center, Davos, Switzerland.
[2]Oeschger Center for Climate Change Research and Institute of Applied Physics, University of Bern, Bern, Switzerland.

Correspondence to: Aebi Christine (christine.aebi@pmodwrc.ch)

Abstract. The thermal infrared cloud camera (IRCCAM) is a prototype instrument that determines cloud fraction continuously during day and nighttime ~~with high temporal resolution. It has been developed and tested at Physikalisch-Meteorologisches Observatorium Davos/World Radiation Center (PMOD/WRC) in Davos, Switzerland. The IRCCAM consists of a commercial microbolometer camera sensitive~~ using measurements of the absolute thermal sky radiance distributions in the 8 μm - 14 μm wavelength range in conjunction with clear sky radiative transfer modelling. Over a time period of two years, the fractional cloud coverage obtained by the IRCCAM is compared with two other commercial cameras ~~sensitive in the visible spectrum~~ (Mobotix Q24M and Schreder VIS-J1006) sensitive in the visible spectrum, as well as with the automated partial cloud amount detection algorithm (APCADA) using pyrgeometer data. ~~In comparison to the visible cloud detection algorithms, the IRCCAM shows median difference values of 0.01 to 0.07 cloud fraction wherein around 90 % of the data are within ±0.25 (±~~Over the two year period, the cloud fractions determined by the IRCCAM and the visible sky cameras are consistent to within 2 oktas ~~) cloud fraction. Thus there is no significant difference in the cloud fraction determination of the IRCCAM in comparison to the other study instruments. Analysis indicates no significant difference in the performance of the IRCCAM during day or nighttime and also not in different seasons. The cloud types where all algorithms are in closest agreement are low-level clouds (with median differences in cloud fraction of -0.01 to 0.02), followed by mid-level (0.00) and high-level clouds (-0.13)~~0.25 cloud fraction) for 90 % of the dataset during the day while for day- and nighttime data the comparison with the APCADA algorithm yields an agreement of 80 %. These results are independent of cloud types with the exception of thin cirrus clouds which are not detected as consistently by the current cloud algorithm of the IRCCAM. The measured absolute sky radiance distributions also provide the potential for future applications such as cloud emissivity by combining these measurements with ancillary meteorological data from radiosondes and ceilometers.

1 Introduction

Clouds affect the surface radiation budget and thus the climate system on a local as well as on a global scale. Clouds have an influence on solar and on terrestrial radiation by absorbing, scattering and emitting radiation. The Intergovernmental Panel on Climate Change (IPCC) states that clouds in general and aerosol-cloud interactions in particular generate considerable uncertainty in climate predictions and climate models (IPCC, 2013). ~~Information about cloud coverage~~ Having information about

cloud fraction on a local scale is of importance ~~not only in climate topics, but also in the production of electricity, because coverage of the sun with clouds leads to a reduction of energy production from photovoltaic panels (Parida et al., 2011)~~in different fields: for solar power production due to the fact that clouds cause a large variability in the energy production (Parida et al., 2011; Mateos et al., 2014; Tzoumanikas et al., 2016), for aviation and weather forecast or microclimatological

5   studies.

The most common practice ~~globally~~ worldwide to determine cloud coverage, cloud base height (CBH) and cloud type ~~is human observation~~ from the ground are human observations (CIMO, 2014). These long-term series of cloud data allow climate studies to be conducted (e.g. Chernokulsky et al., 2017). Cloud detection by human observers ~~has the advantage that the observations are~~ is carried out several times per day over a long time period ~~and that it is independent of any technical failure~~

10   without the risk of a larger data gap due to a technical failure of an instrument. However, ~~there is no reference standard~~ even with a reference standard defined by the World Meteorological Organisation (WMO) for human observers~~and thus~~, the cloud determination is not objective e.g. mainly due to varying degrees of experience (Boers et al., 2010). Other disadvantages of human ~~observers~~ cloud observations are that the temporal resolution is coarse and due to visibility issues nighttime determinations are difficult. Since clouds are highly variable in space and time, measurements at high spatial and temporal resolution

15   with small ~~measurement~~ uncertainties are needed ~~. Research in the recent past~~ (WMO, 2012). Recent research has therefore been conducted ~~in order~~ to find an automated cloud detection instrument (or a combination of such) to replace human observers ~~(Boers et al., 2010; Tapakis and Charalambides, 2013)~~(Boers et al., 2010; Tapakis and Charalambides, 2013; Huertas-Tato et al., 2017; Sm .

~~One alternative to synoptic~~ An alternative to detect clouds from the ground by human observations is to detect ~~clouds with~~

20   ~~satellites~~them from space. With a ~~time resolution of~~ temporal resolution of 5 to 15 minutes, Meteosat Second Generation (MSG) geostationary satellites are able to detect cloud coverage with a higher time resolution than ~~it~~is accomplished by human observers (Ricciardelli et al., 2010; Werkmeister et al., 2015). ~~Additionally, satellites cover a~~The geostationary satellite Himawari-8 (Da, 2015) even delivers cloud information with a temporal resolution of 2.5 to 10 minutes and a spacial resolution of 0.5 to 2 km. However, these geostationary satellites cover only a certain region of the globe. Circumpolar satellites (i.e.

25   the MODIS satellites Terra and Aqua (Baum B.A., 2006; Ackerman et al., 2008)) determine cloud fraction globally, but for a specific region only four times a day. Satellites cover a larger area than ground-based instruments and ~~global coverage of cloud information is possible.~~are also able to deliver cloud information from regions where few ground-based instruments are available (e.g. in Arctic regions (Heymsfield et al., 2017) or over oceans). However, due to the large field of view (FOV) of satellites, small clouds can be overlooked ~~and thin clouds cannot be distinguished from land (Dybbroe et al., 2005; Calbo and Sabburg, 200~~

30   (Ricciardelli et al., 2010). Another challenge with satellite data is the ability to distinguish thin clouds from land (Dybbroe et al., 2005; Acke . Furthermore, satellites collect information mainly from the highest cloud layer rather than the lower cloud layer closer to the ~~Earth~~earth's surface. ~~In order to retrieve information about the lower cloud levels, measurements from the ground are required.~~Nowadays satellite data are validated and thus supported by ground-based cloud data. Different studies focusing on the comparison of the determined cloud fraction from ground and from space were presented by e.g. Fontana et al. (2013); Wacker et al. (2015);

35   .

In general, three ~~automatic~~ ground-based cloud ~~cover~~ measurement techniques are distinguished: radiometers, active column instruments and hemispherical sky cameras. Radiometers measure the incident radiation in different wavelength ranges. ~~In the presence of clouds, depending~~ Depending on the wavelength range, the presence of clouds alters the radiation measured at ground level ~~is lower or higher than without clouds (e.g. Calbo et al., 2001; Mateos Villàn et al., 2010). The FOV of some~~

5 ~~of these radiometersis rather small. Some of these instruments , such as~~ (e.g. Calbo et al., 2001; Mateos Villàn et al., 2010). Calbo et al. (2001) and Dürr and Philipona (2004) both present different methodologies to determine cloud conditions from broadband radiometers. Other groups describe methodologies using instruments with a smaller spectral range. Such instruments are for example the infrared pyrometer CIR-7 (Nephelo) (Tapakis and Charalambides, 2013) or Nubiscope ~~(Boers et al., 2010; Feister et al., ,~~ (Boers et al., 2010; Feister et al., 2010; Brede et al., 2017), which both measure in the 8 μm - 14 μm wavelength range of the

10 spectrum. In order to retrieve cloud information~~of the whole upper hemisphere~~, Nephelo consists of seven radiometers which scan the ~~sky~~whole upper hemisphere. The Nubiscope consists of one radiometer only, which also scans the whole upper hemisphere. Such a scan takes several minutes, which is a limitation on the retrieval of cloud fraction information when for example fast-moving clouds occur (Berger et al., 2005). In general, these instruments give information about cloud fraction for three different levels, cloud types and cloud base height (CBH) (Wauben, 2006). Brocard et al. (2011) presents a method using data

15 from the tropospheric water vapour radiometer (TROWARA) to determine cirrus clouds from the measured fluctuations in the sky infrared brightness temperature.

The ~~active cloud measurement~~ second group, the column cloud detection instruments send a laser pulse to the ~~sky~~ atmosphere and measure the ~~reflected~~ backscattered photons. The photons are scattered back by hydrometeors in clouds and, depending on the time and the amount of ~~reflected~~ backscattered photons measured, the cloud base height can be determined. However, the

20 laser pulse is not only scattered back by cloud hydrometeors, but also by aerosols (Liu et al., 2015). Examples of active remote sensing instruments are ~~radars (Kato et al., 2001; Feister et al., 2010), lidars~~ cloud radar (Kato et al., 2001; Illingworth et al., 2007; Feister , lidar (Campbell et al., 2002; Zhao et al., 2014) and ceilometers (Martucci et al., 2010). ~~The~~ Due to the narrow beam, a disadvantage of these ~~measurements~~ measurement techniques is the lack of ~~information about the whole sky. Thus, with for example ceilometers, a fully covered or cloud-free sky is detected with considerable accuracy, however, the detection of~~

25 ~~oktas~~ instantaneous cloud information of the whole upper hemisphere. Boers et al. (2010) showed that with smaller integration times the instruments tend to give okta values of zero and eight rather than the intermediate cloud fractions of 1 to 7~~is more difficult (Boers et al., 2010)~~ oktas.

The third group of ground-based cloud detection instruments comprises the hemispherical sky cameras, which have a 180° view of the upper hemisphere. The most common all-sky ~~cameras are the~~ camera is the commercially available total sky

30 imager (TSI) (Long et al., 2006)~~and~~. Another pioneering hemispherical cloud detection instrument is the whole sky imager (WSI) (Shields et al., 2013). Whereas the TSI is sensitive in the visible spectrum, the WSI acquires information in seven different spectral ranges in the visible and in the near infrared regions. A special version of the WSI also allows nighttime measurements (Feister and Shields, 2005). Other cloud research has been undertaken with low-cost commercial cameras ~~(e.g. Calbo and Sabburg, 2008; Cazorla et al., 2008; Kazantzidis et al., 2012; Wacker et al., 2015)~~sensitive in the visible

35 spectrum of the wavelength range (e.g. Calbo and Sabburg, 2008; Cazorla et al., 2008; Kazantzidis et al., 2012; Wacker et al., 2015; Kuhn

. All these hemispherical sky cameras operate well during daytime, but give no information during nighttime. Thus, there is increasing interest in ~~deployment~~ development of cloud cameras sensitive in the thermal infrared region of the spectrum. Ground-based thermal infrared all-sky cameras have the advantage of delivering continuous information about cloud coverage, cloud base height and cloud type during day and nighttime, which in turn is of interest ~~for climate studies~~in various fields.

5 The infrared cloud imager (ICI) is a ground-based sky camera sensitive in the 8 μm - 14 μm wavelength range and with a resolution of 320 $\times$ 240 pixels (Shaw et al., 2005; Thurairajah and Shaw, 2005; Smith and Toumi, 2008). ~~The~~ Another instrument, the Solmirus all-sky infrared visible analyser (ASIVA) ~~has been presented by Klebe et al. (2014). ASIVA~~ consists of two cameras, one measuring in the visible and the other one in the 8 μm - 13 μm wavelength range (Klebe et al., 2014). The whole-sky infrared cloud measuring system (WSIRCMS) ~~(Liu et al., 2013)~~ is an all-sky cloud camera sensitive in the 8 μm - 14 μm

10 wavelength range ~~, which~~ (Liu et al., 2013). The WSIRCMS consists of nine cameras measuring at the zenith and at eight surrounding positions. With a time resolution of 15 minutes, information about cloud cover, CBH and cloud type are determined. This instrument has an accuracy of $\pm$0.3 oktas compared to visual observations (Liu et al., 2013). Redman et al. (2018) presented a reflective all-sky imaging system (sensitive in the 8 μm - 14 μm wavelength range) consisting of a longwave infrared microbolometer camera and a reflective sphere (110° FOV). Relatively new on the market is the Sky Insight thermal

15 infrared cloud imager from Reuniwatt. The Sky Insight cloud imager is sensitive in the 8 μm - 13 μm wavelength range and its layout and software is similar to the prototype instrument presented here.

The current study describes a newly developed instrument, the thermal infrared cloud camera (IRCCAM), that consists of a modified commercial thermal camera ~~that gives~~ (Gobi-640-GigE) that gives instantaneous information about cloud conditions ~~with a 180° FOV and a~~ for the full upper hemisphere. The time resolution of the IRCCAM in the current study is

20 1 minute during day- and nighttime. It measures in the wavelength range of 8 μm - 14 μm. The IRCCAM has been in use at the Physikalisch-Meteorologisches Observatorium Davos/World Radiation Center (PMOD/WRC), Davos, Switzerland, since September ~~2015 and is measuring continuously day and night.~~ 2015. The IRCCAM was developed to provide instantaneous hemispheric cloud coverage information from the ground with a high temporal resolution in a more objective way than human cloud observations. Thus the IRCCAM could be used for different applications at meteorological stations, at airports or at

25 solar power plants. The performance of the IRCCAM regarding cloud fraction is compared with data from two visible all-sky cameras and the automatic partial cloud amount detection algorithm (APCADA) (Dürr and Philipona, 2004). In section 2, the instruments and cloud detection algorithms are presented. The comparison of the calculated cloud fractions based on different instruments and algorithms are analysed and discussed overall and for different cloud classes, times of day ~~, seasons and cloud classes~~ and seasons separately in section 3. Section 4 provides a summary and conclusions.

30 ## 2 Data and Methods

All three all-sky camera systems used for the current study are installed at the Physikalisch-Meteorologisches Observatorium Davos/World Radiation Center (PMOD/WRC), Davos, located in the Swiss Alps (46.81°N, 9.84°E, 1,594 m asl). There are two commercial cameras, one ~~from Mobotix AG~~ Q24M from Mobotix and the other ~~from Schreder GmbH, both~~ is a J1006 cloud

camera from the company Schreder. Both of these cameras are measuring in the visible spectrum~~, and a~~. The third camera is the newly developed all-sky camera (IRCCAM) sensitive in the thermal infrared wavelength range~~from 8 μm - 14 μm~~. The instruments themselves and their respective analysis software are described in the following subsections. Also, the automatic partial cloud amount detection algorithm (APCADA) is briefly described in Section 2.4.

5 The analysis of the data from the thermal infrared cloud camera (IRCCAM) is performed for the time period September 21, 2015 to September 30, 2017, with a ~~sizeable~~ data gap between December 20, 2016 and February 24, 2017 due to maintenance of the instrument. Mobotix and APCADA data are available for the whole aforementioned time period. Schreder data are only available since March 9, 2016. Thus the analysis of these data is only performed for the time period March 9, 2016 to September 30, 2017.

2.1 Thermal infrared cloud camera

The Infrared Cloud Camera (IRCCAM) (Figure 1) consists of a commercial thermal infrared camera (Gobi-640-GigE) from Xenics (www.xenics.com). The camera is an uncooled microbolometer sensitive in the wavelength range of 8 μm - 14 μm. The chosen focal length of the camera objective is 25 mm and the field of view $18° \times 24°$. The image resolution is 640×480 pixels. The camera is located on top of a frame looking downward on a gold-plated spherically shaped aluminium mirror such

15 that the entire upper hemisphere is imaged on the camera sensor. The complete system is 1.9 m ~~high and the~~ tall. The distance between the camera objective and the mirror is about 1.2 m. These dimensions were chosen in order to reflect the radiation from the whole upper hemisphere onto the mirror and to minimise the area of the sky hidden by the camera itself. The arm holding the camera above the mirror is additionally fixed with two wire ropes to stabilise the camera ~~against wind~~during windy conditions. The mirror is gold-plated to reduce the emissivity of the mirror and to make ~~measurement~~ measurements of the

20 infrared sky radiation largely insensitive to the mirror temperature. Several temperature probes are included to monitor the mirror, camera and ambient temperatures.

The camera of the IRCCAM was calibrated in the ~~laboratory of~~ PMOD/WRC laboratory in order to determine the brightness temperature or the absolute radiance in Wm^{-2}sr^{-1} for every pixel in an IRCCAM image. The absolute calibration was obtained by placing the camera in front of the aperture of a well characterised blackbody at a range of known temperatures between

25 -20 °C and +20 °C in steps of 5 °C (Gröbner, 2008). The radiance emitted by a blackbody radiator can be calculated using the Planck radiation formula,

$$L_\lambda(T) = \frac{2hc^2}{\lambda^5} \frac{1}{e^{\frac{hc}{k\lambda T}} - 1} \tag{1}$$

where T is the temperature, λ the wavelength, h is the Planck constant, 6.6261×10^{-34} Js, c the speed of light, 299'792'458 ms^{-1} and k the Boltzmann constant, 1.3806×10^{-23} J K^{-1}. For the IRCCAM camera, ~~assuming a nominal spectrally flat response~~

30 ~~between 8 μm and 14 μm, this yields,~~ the spectral response function R_λ as provided by the manufacturer is shown in Figure 2 and is used to calculate the integrated radiance L_R,

$$L_{8-14R} = \int_8^{1425} R_\lambda \cdot L_\lambda(T) d\lambda \tag{2}$$

5

where T is the effective temperature of the blackbody (Gröbner, 2008) and ~~L_{8-14}~~ L_R the integrated radiance measured by the IRCCAM camera. To retrieve the brightness temperature (T_B) from the integrated radiance ~~L_{8-14}~~ L_R, Eq. 2 cannot be solved analytically. Therefore, as an approximation, we are using a polynomial function ~~$T_B = f(L_{8-14})$~~ $T_B = f(L_R)$ to retrieve the brightness temperature T_B from the radiance ~~L_{8-14}~~ L_R. Using Eq. 2, ~~L_{8-14}~~ L_R values are calculated for temperatures in the

5   range of -40 °C and +40 °C ~~assuming a nominal spectrally flat response function of the IRCCAM~~. The resulting fitting function is a polynomial ~~function third order~~ third order function (see Figure 3), which is ~~thereafter~~ used to retrieve T_B from the integrated radiance ~~L_{8-14}~~ L_R for every pixel in an IRCCAM image.

The IRCCAM calibration in the blackbody aperture was performed on March 16, 2016 and all its images are calibrated with the corresponding calibration function retrieved from the laboratory measurements. The calibration uncertainty of the camera

10   in terms of brightness temperatures (in a range of -40 °C and +40 °C) is estimated at 1 K for a Planck spectrum as emitted by a blackbody radiator. Furthermore, a temperature correction function for the camera was derived from these laboratory calibrations in order to correct the measurements obtained at ambient temperatures outdoors.

The hemispherical sky images taken by the IRCCAM are converted to polar coordinates (Θ, Φ) for the purpose of retrieving brightness temperatures in dependence of zenith and azimuth respectively. Due to slight aberrations in the optical system of the

15   IRCCAM, the Θ coordinate does not follow a linear relationship with the sky zenith angle, producing a distorted sky image. Therefore, a correction function was determined by correlating the apparent solar position as measured by the IRCCAM with the true solar position obtained by a solar position algorithm. This correction function was then applied to the raw camera images to obtain undistorted images of the sky hemisphere.

One should note that observing the sun with the Gobi camera implies that the spectral filter used in the camera to limit the

20   spectral sensitivity to the 8 μm - 14 μm wavelength band has some leakage at shorter wavelengths. Fortunately, this leakage is confined to a narrow region around the solar disk (around 1°) as shown in Figure 4. Thus it has no effect on the remaining part of the sky images taken by the IRCCAM during daytime measurements.

The main objective of the IRCCAM study is to determine cloud properties from the measured sky radiance distributions. The cloudy pixels in every image are determined from their observed higher radiances with respect to that of a cloud-free sky. The

25   clear sky radiance distributions are determined from radiative transfer calculations using MODTRAN 5.1 (Berk et al., 2005), using as input parameters screen-level air temperature and integrated water vapour (IWV). The temperature was determined at 2 m elevation obtained from a nearby SwissMetNet station, while the IWV was retrieved from GPS signals operated by the Federal Office for Topography and archived in the Studies in Atmospheric Radiation Transfer and Water Vapour Effects (STARTWAVE) database hosted at ~~IAP,~~ the Institute of Applied Physics at the University of Bern (Morland et al., 2006). For

30   practical reasons, a lookup table (LUT) for a range of temperatures and IWV was generated which was then used to compute the reference clear sky radiance distribution for every single image taken by the camera.

The sky brightness temperature distribution as measured on a cloud-free day (June 18, 2017 10:49 UTC) and the corresponding modelled sky brightness temperature are shown in Figure 4a and Figure 4b, respectively. As expected, the lowest radiance is emitted at the zenith, with a gradual increase at increasing zenith angle, until the measured effective sky brightness temperature

35   at the horizon is nearly equal to ambient air temperature (Smith and Toumi, 2008). Figure 4c shows the profiles of the measured

~~and modelled~~ (red) and modelled (blue) brightness temperatures along one azimuth position going through the solar position (yellow line in Figure 4a). As can be seen in Figure 4c, the measured and modelled sky distributions agree fairly well, with large deviations at high zenith angles due to the mountains obstructing the horizon around Davos. The shortwave leakage from the sun can also be clearly seen around pixel number ~~180 and a smaller deviation~~ 180. A smaller deviation is seen at pixel

5 number 239 from the wires holding the frame of the camera.

The average difference between the measured and modelled clear sky radiance distributions was determined for several clear sky days during the measurement period in order to use that information when retrieving clouds from the IRCCAM images. Such differences can arise on the one hand from the rather crude radiative transfer modelling which ~~uses~~ only uses surface temperature and IWV as input parameters to the model~~only surface temperature and IWV, and on~~. On the other hand it can

10 arise from instrumental effects such as a calibration uncertainty of ± 1 K~~, the~~. An effect of the mirror temperature ~~which has not been taken into account,~~ and a possible mismatch between actual and nominal spectral response functions of the IRCCAM camera ~~,~~ are other potential causes for this difference. But both of these possible effects have not been taken into account. The validation measurements span 8 days, with full sky measurements obtained every minute, yielding a total of 11,512 images for the analysis. For every image, the corresponding sky radiance distribution was calculated from the LUT, as shown in Figure 4b.

15 The residuals between the measured and modelled sky radiance distributions were calculated by averaging over all data points with zenith angles smaller than $60°$, while removing the elements of the IRCCAM within the field of view of the camera (frame and wires), resulting in one value per image. The brightness temperature differences between IRCCAM and model calculations show a mean difference of +4.0 K and a standard deviation of 2.4 K over the whole time period. The observed variability comes equally from ~~day to day~~ day-to-day variations as well as from variations within a single day. No systematic

20 differences are observed between day and nighttime data.

The stability of the camera over the measurement period is investigated by comparing the horizon brightness temperature derived from the IRCCAM with the ambient air temperature measured at the nearby SwissMetNet station. As mentioned by Smith and Toumi (2008), the horizon brightness temperature derived from the IRCCAM should approach the surface air temperature close to the horizon. Indeed, the average difference between the horizon brightness temperature derived from the

25 IRCCAM and the surface air temperature was 0.1 K with a standard deviation of 2.4 K, showing no drifts over the measurement period ~~,~~ and thus confirming the good stability of the IRCCAM during this period. The good agreement of 0.1 K between the derived horizon brightness temperature from the IRCCAM and the surface air temperature confirms the absolute calibration uncertainty of ± 1 K of the IRCCAM. Therefore, the observed discrepancy of 4 K between measurements and model calculations mentioned previously can probably be attributed to the uncertainties in the model parameters (temperature and IWV)

30 used to produce the LUT.

2.1.1 Cloud detection algorithm

After setting up the IRCCAM, a horizon mask is created initially to determine the area of the IRCCAM image representing the sky hemisphere. A ~~clear sky~~ cloud-free image is selected manually~~, and the~~. The sky area is selected by the very low sky brightness temperatures with respect to the local obstructions with much larger brightness temperatures. This image mask

contains local obstructions such as the IRCCAM frame (camera, arm and wire ropes) as well as the horizon, which in the case of Davos consists of mountains limiting the field of view of the IRCCAM. Thereafter, the same horizon mask is applied to all IRCCAM images. The total number of pixels within the mask is used as a reference and the cloud fraction is defined as the number of pixels detected as cloudy relative to the total number.

The algorithm to determine cloudy pixels from an IRCCAM image consists of two parts. The first part uses the clear sky model calculations as a reference to retrieve low to mid-level clouds. These clouds have large temperature differences compared to the clear sky reference. In this part of the algorithm, cloudy pixels are defined for measured sky brightness temperatures that are at least 6.5 K greater than the modelled clear-sky reference value. A rather large threshold value was empirically chosen to avoid any erroneous clear sky mis-classifications as cloudy pixels. The thinner and higher clouds with lower brightness temperatures are therefore left for the second part of the algorithm.

In order to determine the thin and high-level clouds within an IRCCAM image, non cloudy pixels remaining from the first part of the algorithm are used to fit an empirical clear sky brightness temperature as a function of the zenith angle,

$$T_B = (T_{65} - a)(\frac{\Theta}{65})^b + a \tag{3}$$

where T_B is the brightness temperature for a given zenith angle Θ, and T_{65}, a and b are the retrieved function parameters (Smith and Toumi, 2008). This second part of the algorithm assumes a smooth variation of the clear sky brightness temperature with zenith angle. Thereby it determines cloudy pixels as deviations from this smooth function as well as requiring a brightness temperature higher than this empirical clear sky reference. Pixels with a brightness temperature higher than the empirically defined threshold of 1.2 K are defined as cloudy and removed from the clear sky data set. This procedure is repeated up to 10 times to iteratively find pixels with a brightness temperature higher than the clear sky function. One restriction of this fitting method is that it requires at least broken cloud conditions, as it does not work well under fully overcast conditions without the presence of any cloud-free pixels to constrain the fitting procedure.

The selected threshold of 1.2 K allows the detection of low emissivity clouds, but still misses the detection of thin, high-level cirrus clouds even though they can be clearly seen in the IRCCAM images. Unfortunately, reducing the threshold to less than 1.2 K results in many clear sky mis-classifications as clouds. Therefore under these conditions, it seems that using a spatial smoothness function is not sufficient to infer individual pixels as being cloudy; a more advanced algorithm as discussed in Brocard et al. (2011) is required to define clouds not only on a pixel by pixel basis but as a continuous structure (e.g. pattern recognition algorithm).

Before reaching the final fractional cloud data set, some data filtering procedures are applied: situations with precipitation are removed by considering precipitation measurements from the nearby SwissMetNet station; ice or snow deposition on the IRCCAM mirror is detected by comparing the median radiance of a sky area with the median radiance value of an area on the

image showing the frame of the IRCCAM. In cases where the difference between the median values of the two areas is smaller than the empirically defined value of 5 $\text{Wm}^{-2}\text{sr}^{-1}$, the mirror is assumed contaminated by snow or ice and therefore does not reflect the sky, so the image is excluded. The horizon mask does not cover all pixels that do not depict sky, which leads to an offset in the calculated cloud fraction of around 0.04. This offset is removed before comparing the cloud fraction determined by the IRCCAM with other instruments.

2.2 Mobotix camera

A commercial surveillance Q24M camera from Mobotix (www.mobotix.com) has been installed in Davos since 2011. The camera has a fisheye lens and is sensitive in the red-green-blue (RGB) wavelength range. The camera takes images from the whole upper hemisphere with a spatial resolution of 1200×1600 pixels. The camera system is heated, ventilated and installed on a solar tracker with a shading disk. The shading disk avoids overexposed images due to the sun. The time resolution of the Mobotix data is one minute (from sunrise to sunset) and the exposure time is 1/500 s.

An algorithm determines the cloud fraction of each image automatically (Wacker et al., 2015; Aebi et al., 2017). Before applying the cloud detection algorithm, the images are preprocessed. The distortion of the images is removed by applying a correction function. ~~A~~ The same horizon mask, which ~~is~~ was defined on the basis of a cloud-free image, is applied to all images. After this preprocessing, the colour ratio (the sum of the blue to green ratio plus the blue to red ratio) is calculated per pixel. To perform the cloud determination per pixel, this calculated colour ratio is compared to an empirically defined reference ratio value of 2.2. Comparing the calculated colour ratio value with this reference value designates whether a pixel is classified as ~~a cloudy pixel or as a~~ cloudy or as cloud-free ~~pixel~~. The cloud fraction is calculated by the sum of all cloud pixels divided by the total number of sky pixels.

The cloud classes are determined with a slightly adapted algorithm from Heinle et al. (2010) which is based on statistical features (Wacker et al., 2015, Aebi et al., 2017). The cloud classes determined are stratocumulus (Sc), cumulus (Cu), stratus-altostratus (St-As), cumulonimbus-nimbostratus (Cb-Ns), cirrocumulus-altocumulus (Cc-Ac), cirrus-cirrostratus (Ci-Cs) and cloud-free (Cf).

2.3 Schreder camera

The total sky camera J1006 from Schreder ~~GmbH~~ (www.schreder-cms.com) consists of a digital camera with a fisheye lens. The J1006 Schreder camera is sensitive in the RGB region of the spectrum and takes two images every minute with different exposure times (1/500 s and 1/1600 s, respectively). The aperture is fixed at f/8 for both images. The resolution of the images is 1200×1600 pixels. The camera comes equipped with a weatherproof housing and a ventilation system.

The images from the Schreder camera are analysed using two different algorithms. The original software is directly delivered from ~~Schreder GmbH~~ the company Schreder. Before calculating the fractional cloud coverage, ~~the images are preprocessed~~ some steps are needed to define the settings that are needed to preprocess the images. In a first step, the centre of the image is defined manually. In a second step, the maximum zenith angle of the area taken into account for further analyses is defined. Unfor-

tunately, the maximum possible zenith angle is only 70° and thus a larger fraction of the sky cannot be analysed. After the distortion of the images is removed, in a fourth step a horizon mask is defined on the basis of a cloud-free image. The mask also excludes the pixels around the sun. In a last step, a threshold is defined which specifies whether a pixel is classified ~~as cloud or no cloud.~~ or not classified as a cloud. The settings from all these preprocessing steps are then applied to all images

5 from the Schreder camera. In the following, the term Schreder refers to data where this algorithm is used.

Due to the Schreder algorithm's limitation of a maximum zenith angle of 70°, we ~~applied~~ used the same algorithm as ~~the one~~ for the Mobotix camera~~to the Schreder camera images also (thereafter referred to~~, referred hereafter as Schreder$_{pmod}$~~)~~. The algorithm Schreder$_{pmod}$ has the advantage that the whole upper hemisphere is considered when calculating the fractional cloud coverage. Thus, a new horizon mask is defined on the basis of a cloud-free image~~and the~~. The colour ratio reference to

10 distinguish between clouds and no clouds ~~and~~ is assigned an empirical value of 2.5, which is slightly different ~~from the one~~ to that used for the Mobotix camera. The Schreder camera in Davos has been measuring continuously since March 2016.

2.4 APCADA

The automated partial cloud amount detection algorithm (APCADA) determines the cloud amount in oktas using downward longwave radiation from pyrgeometers, temperature and relative humidity measured at screen-level height (Dürr and Philipona,

15 2004). APCADA is only able to detect low- and mid-level clouds and is not sensitive to high-level clouds. The time resolution of APCADA is 10 minutes during day and nighttime. The agreement of APCADA compared to synoptic observations at high-altitude and midlatitude stations, such as Davos, is that 82 % to 87 % of cases during day and nighttime have a maximum difference of ±1 okta (±0.125 cloud fraction) and between 90 % to 95 % of cases have a difference of ±2 oktas (± ~~0.25~~ 0.250 cloud fraction) (Dürr and Philipona, 2004).

20 In order to compare the cloud coverage information retrieved from APCADA with the fractional cloud coverages retrieved from the cameras, the okta values are converted to fractional cloud coverage values by multiplying the okta values ~~with~~ by 0.125.

In the current study, APCADA is mainly used for comparisons of the nighttime ~~data of the IRCCAM~~ IRCCAM data.

3 Results

25 In the aforementioned time period September 21, 2015 to September 30, 2017, the IRCCAM data set comprises cloud cover information from 581,730 images. The Mobotix data set comprises 242,249 images (because only daytime data are available) and the Schreder data set 184,746 images (shorter time period and also only daytime). Figure 5 shows the relative frequencies of cloud cover detection from the different camera systems in okta bins. Zero okta corresponds to a cloud fraction of 0 to 0.05 and 8 oktas to a cloud fraction of 0.95 to ~~1 (Wacker et al., 2015). One to~~ 1. One and seven oktas correspond to intermediate

30 bins of 0.1375 cloud fraction and oktas two to six to intermediate bins of 0.125 cloud fraction (Wacker et al., 2015). Cloud-free (0 okta) and overcast (8 oktas) are the cloud coverages that are most often detected in the aforementioned time period. This behaviour also agrees with the analysis of the occurrence of fractional cloud coverages over a longer time period in Davos

discussed in Aebi et al. (2017). All four instruments show a similar relative occurrence of cloud coverages of 2 - 6 oktas. It is noteworthy that the IRCCAM ~~is clearly underestimating~~ clearly underestimates the occurrence of 0 oktas in comparison to the cameras measuring in the visible spectrum (by up to 13 %). On the other hand, the relative frequency of the IRCCAM of 1 okta is clearly larger (by up to 10 %) compared to the visible cameras. This can be explained by higher brightness temper-

5   atures measured in the vicinity of the horizon ~~which~~ above Davos. These higher measured brightness temperatures are falsely determined as cloudy pixels (up to 0.16 cloud fraction). Since these situations with larger brightness temperatures occur quite frequently, the IRCCAM algorithm ~~determines as clouds~~ detects more often cloud coverages of 1 okta instead of 0 okta. Also, at the other end of the scale, the IRCCAM is detecting slightly larger values of a relative frequency of 7 oktas compared to the visible cameras and slightly lower relative frequencies of a measurement of 8 oktas.

10   As an example, Figure 6 shows the cloud fraction determined on April 4, 2016, where various cloud types and cloud fractions were present. This day starts with an overcast sky and precipitation and therefore the IRCCAM is measuring fractional cloud coverages of more than 0.98. The cloud layer ~~dissolves~~ disperses until it reaches cloud fraction values of 0.1 at around 6 UTC. At this time the sun rises above the effective horizon and the visible all-sky cameras start to measure shortly thereafter. The cloud classes are determined with the algorithm developed by Wacker et al. (2015) based on Mobotix images. In the early

15   morning, the cloud type present is cumulus. The larger difference of more than 0.1 between the cloud fraction determined by the Schreder algorithm and the other algorithms can be explained after a visual observation of the image: the few clouds that are present are located ~~in close proximity~~ close to the horizon and thus in the region of the sky that the Schreder algorithm is not able to analyse. The fractional cloud coverage increases again to values of around 0.8 at 7 UTC. At this time, all four cameras and algorithms determine a similar fractional cloud coverage. Around 8 UTC a first cirrostratus-layer appears which is

20   slightly better detected by the IRCCAM and the Mobotix algorithm than by the two algorithms using the Schreder images. Two hours later, around 10 UTC, the main cloud type present is again cumulus. Low-level clouds are quite precisely detected by all camera systems and thus, in this situation, the maximum observed difference is only ~~0.07~~0.06. Figure 7a shows exactly this situation as an RGB-image taken by the Mobotix camera, and the corresponding classifications as cloudy or non-cloudy pixels determined by the IRCCAM (Figure 7b) and by the Mobotix algorithm (Figure 7c). From 11 UTC onwards the cumulus clouds

25   are found in the vicinity of the horizon and cirrus-cirrostratus closer to the zenith. Because ~~the detection of~~ all algorithms have difficulties to detect thin and high-level clouds~~is difficult for all algorithms~~, the differences in the determined cloud fractions are variable. Again, the Schreder algorithm is not able to analyse the cloud fraction near the horizon and thus it always detects the smallest fraction compared to the other algorithms. The visible cameras continue measuring until 16:23 UTC when the sun sets and afterwards only data from the IRCCAM are available.

30

3.1   Visible all-sky cameras

Before validating the fractional cloud coverage determined by the IRCCAM algorithm, the fractional cloud coverages, which are determined using the images of the visible all-sky cameras Mobotix and Schreder, are compared among each other to gain a better understanding of their performance. The time period analysed here is March 9, 2016 to September 30, 2017, consisting

of only daytime data, which corresponds to a data set of 184,746 images. Additionally, the results from the visible all-sky cameras are compared with data retrieved from APCADA (temporal resolution of 10 min). For this comparison, 32,902 and 24,907 Mobotix and Schreder images respectively are considered.

The histograms of the residuals of the difference in the cloud fractions (range between [-1;1]) between the visible all-sky cameras are shown in Figure 8 and the corresponding median and 5th and 95th percentiles are shown in Table 1.

As shown in Table 1, the two algorithms from the Schreder camera as well as APCADA underestimate the cloud fraction determined from Mobotix images, with a maximum median difference of -0.04. Although the median difference in cloud fraction between the two Schreder algorithms is 0.00, the distribution tends towards more negative values. This more pronounced underestimation of fractional cloud coverage of the Schreder algorithm might be explained by ~~its~~ the smaller fraction of the sky being analysed (Figure 8c). The underestimation in the retrieved cloud fraction of the Schreder algorithm for 90 % of the data is even slightly larger in comparison to the cloud fraction determined with the Mobotix algorithm. The spread (shown as 5th and 95th percentiles in Table 1) is greatest for all comparisons of the algorithms from the visible cameras with APCADA. As previously mentioned in Section 2.4, APCADA gives the cloud fraction only in steps of 0.125~~cloud fraction~~, and is thus not as accurate as the cloud fraction determined from the cameras~~, which~~. This fact might explain the large variability in the residuals.

In Figure 8 it is shown that the distribution of the residuals between the cloud fraction retrieved from Mobotix versus the cloud fraction retrieved from the two Schreder algorithms (Figure 8a and 8b) are left-skewed, which confirms that the cloud fraction retrieved from the two Schreder algorithms underestimates the cloud fraction retrieved from the Mobotix images.

Taking the measurement uncertainty of human observers and also of other cloud detection instruments to be ± 1 okta to ± 2 oktas (Boers et al., 2010), we take this as a baseline uncertainty range to test the performance in the detection of cloud fraction of our visible camera systems. The algorithms for the visible camera systems determine the cloud fraction for 94 - 100% of the data within ± 2 okta (± 0.25) and for 77 - 94 % of the data within ± 1 okta (± 0.125). Comparing the cloud fraction determined from APCADA with the cloud fraction determined from the visible cameras shows that in only 62 - 71 % of the cases is there an agreement of ± 1 okta (± 0.125) and in 83 - 86 % of data an agreement of ± 2 okta (± 0.25). All these results are further discussed in ~~Section 3.2.3~~the next Section.

3.2 IRCCAM Validation

As described in Section 3.1, in up to 94 % of the data set the visible cameras ~~do agree~~ are consistent to within $\pm$~~2~~1 okta ($\pm$~~0.25~~0.125) in the cloud fraction detection, so that they can be used to validate the fractional cloud coverage determined by the IRCCAM. For this comparison, a data set of 242,249 images (Mobotix) and a data set of 184,746 images (Schreder) are available. This comparison is only performed for daytime data of the IRCCAM, because from the visible cameras only daytime data are available.

The residuals and some statistical values of the differences between the IRCCAM and the visible cameras are shown in Figure 9 and Table 2. With a median value of 0.01, there is no ~~significant~~ considerable difference between the cloud fraction determined by the IRCCAM and the cloud fraction determined by the Mobotix camera. The differences between the IRCCAM and the

Schreder algorithms are only slightly larger, with median values of 0.04 and 0.07 for Schreder$_{pmod}$ and Schreder respectively. The distributions of the residuals IRCCAM-Schreder and IRCCAM-Schreder$_{pmod}$ are quite symmetrical (Figure 9b and 9c). The distribution of the residuals in cloud fraction IRCCAM-Mobotix is slightly left-skewed. ~~The IRCCAM agrees in up to~~ The percentage of agreement in the determined cloud fraction between the sky cameras and APCADA separately is given in

5 Table 3. All values above the grey cells designate the fraction of data that agree within ±0.125 (±1 okta) fractional cloud coverage between two individual algorithms and all values below the grey cells indicate the fraction that agree within ±0.25 (±2 oktas) cloud fraction.

The agreement of the IRCCAM in comparison with different visible all-sky cameras and APCADA is that 59–77 % of the ~~cases within a difference in cloud fraction of~~ IRCCAM data are within ± 0.125 (±1 okta~~and in even up to~~) fractional cloud

10 coverage and 78 - 93 % of the ~~cases~~ data are within ±~~0.25 (±2 oktas. Thus, in general, we~~) fractional cloud coverage. We can conclude that the IRCCAM retrieves cloud fraction values within the uncertainty range of the cloud fraction retrieved from the visible cameras ~~.~~and also in a similar range as state of the art cloud detection instruments. These values of the IRCCAM are only slightly lower than the agreement that the visible cameras have amongst each other. The close agreement between the two algorithms Schreder and Schreder$_{pmod}$ is noteworthy, although they analyse a different number of pixels of the images.

15

3.2.1   Cloud Class Analysis

Although the median difference between the cloud fraction determined with the IRCCAM algorithm and the cloud fraction determined with the Mobotix algorithm is not ~~significant~~evident, it is interesting to analyse differences in cloud fraction depending on the cloud type. The algorithm developed by Wacker et al. (2015) is used to distinguish six selected cloud classes

20 and cloud-free cases automatically on the basis of the Mobotix images. Figure 10 shows the distribution of the residuals of the cloud fraction of the two aforementioned algorithms for (a) cumulus (low-level; N=37,320), (b) cirrocumulus-altocumulus (mid-level; N=52,097) and (c) cirrus-cirrostratus (high-level; N=10,467). The median value of the difference in cloud fraction between IRCCAM and Mobotix for Cu clouds is 0.02 and therefore ~~statistically not significant~~not considerable. In general, all low-level clouds (Sc, Cu, St-As, Cb-Ns) are detected with a median cloud fraction difference of - 0.01 to 0.02 (Table 4).

25 The IRCCAM and the Mobotix camera observe the mid-level cloud class Cc-Ac with a median agreement of 0.00, but with a slightly asymmetric distribution towards negative values. Considering 90 % of the data set of Cc-Ac clouds, the IRCCAM tends to underestimate the cloud fraction for the mid-level cloud class. The spread in the Cc-Ac data (shown as 5th and 95th percentiles in Table 4) is in general slightly larger than ~~the one~~that for low-level clouds. The median value of the ~~residuals in cloud fraction~~ cloud fraction residuals determined on the basis of IRCCAM images and ~~the ones~~those based on Mobotix

30 images for the high-level cloud class Ci-Cs is, at -0.13, ~~significantly~~ is clearly larger in comparison to clouds at lower levels. Thus, although we applied the second part of the algorithm to detect thin, high-level clouds from the IRCCAM images, it still misses a large fraction of the Ci-Cs clouds in comparison to the Mobotix camera. The distribution (Figure 10c) of the residuals is clearly wider, which leads to 5th and 95th percentiles of -0.42 and 0.21 respectively. Due to the large spread,

and also as shown in Aebi et al. (2017), the visible camera systems also have difficulties in detecting the thin, high-level clouds.

3.2.2 Day-night differences

So far, only daytime data have been analysed. At PMOD/WRC in Davos, during nighttime the cloud fraction is retrieved from pyrgeometers as well as from the IRCCAM. Therefore the IRCCAM cloud coverage data are compared with the data retrieved from the automated partial cloud amount detection algorithm (APCADA), which uses pyrgeometer data ~~, which~~ and calculates cloud fractions independent of the time of day. As explained in Section 2.4, APCADA only determines the cloud fraction from low- to mid-level clouds and gives no information about high-level clouds. It also gives the cloud fraction only in okta-steps (equals steps of 0.125 cloud fraction).

Table 5 shows the median values of the residuals of the cloud fraction between IRCCAM and APCADA for all available data (N=103,635), only daytime data (N=32,902) and only nighttime data (N=70,722) and the corresponding 5th and 95th percentiles separately. The overall median difference value in cloud fraction detection between IRCCAM and APCADA is, at 0.05, in a similar range as the ones for the comparison of the cloud fraction determined with the cloud cameras. The median value for daytime data is, at 0.06, only slightly larger than the one for nighttime data (0.04). However, the spread of the residuals is notably broad mainly during nighttime with a large positive 95th percentile value (0.65). However, because APCADA already showed larger spreads in the residuals in comparison to the fractional cloud coverage determined with the visible all-sky cameras, it is not possible to draw the conclusion that the IRCCAM is overestimating the cloud fraction at nighttime.

3.2.3 Seasonal variations

The seasonal analysis is performed in order to investigate whether a slightly unequal distribution of cloud types in different months in Davos (Aebi et al., 2017) have an impact on the performance of the cloud fraction retrieval between seasons. The percentage of agreement in the ~~determined~~ retrieved cloud fraction between the ~~sky cameras and APCADA separately is given in Table 3. All values above the grey cells designate the fraction of data that agree within~~ systems is again given for maximum $\pm$0.125 ($\pm$1 okta ~~) fractional cloud coverage between two individual algorithms and all values below the grey cells indicate the fraction that agree within $\pm$0.25 ($\pm$2 oktas).The agreement of the IRCCAM in comparison with different visible all-sky cameras and APCADA is that 59–77 % of the IRCCAM data are within $\pm$~~0.125~~fractional cloud coverage ~~()~~ differences (top) and $\pm$~~1 okta) and 78 - 93 % of the data are within~~ $\pm$0.25 ~~fractional cloud coverage~~ ($\pm$2 oktas ($\pm$0.25) differences (bottom) for summer (left values) and winter (right values) ~~and thus in a similar range as state of the art cloud detection instruments. These valuesof the IRCCAM are only slightly lower than the agreement that the visible cameras have among each other. The close agreement between the two algorithms Schreder and Schreder~~pmod~~ is noteworthy, although they analyse a different number of pixels of the images.The same analysis was also performed with respect to the four seasons to analyse whether there are seasonal variations. The summer and winter values are shown~~ in Table 6. For all algorithms there is a slightly closer agreement in the determined cloud fraction in the winter months in comparison to the summer months. In winter, the IRCCAM agrees

with the other cameras in 78 - 83 % of the data within ±0.125 (±1 okta) and as high as 84 - 94 % within ±0.25 (±2 oktas). In summer, the agreement in cloud fraction is only 54 - 71 % of the data within ±0.125 (±1 okta) cloud fraction, but nevertheless, 84 - 91 % of values fall within ±0.25 ~~.~~ (±2 oktas) cloud fraction. The slight difference between the two seasons might be explained by the slightly larger frequency of occurrence of the thin and low-emissivity cloud class cirrocumulus-altocumulus

5   in Davos in summer than in winter (Aebi et al., 2017). Also the values for spring ~~and autumn~~ (MAM) and autumn (SON) are in a similar range as the ones for summer and winter. Thus, the IRCCAM (and also the other camera systems) do not show any ~~significant~~ noteworthy variation in any of the seasons.

4   Conclusions

10   The current study describes a newly developed instrument - the thermal infrared cloud camera (IRCCAM) and its algorithm - to determine cloud fraction on the basis of ~~brightness temperature~~ absolute sky radiance distributions. The cloud fraction determined on the basis of IRCCAM images is compared with the cloud fraction determined on the basis of images from two ~~different~~ visible camera systems (one analysed with two different algorithms) and with the partial fractional cloud amount determined with APCADA.

15   The overall ~~agreement of~~ median differences between the determined cloud fraction from the IRCCAM ~~with~~ and the fractional cloud coverage determined from other instruments and algorithms ~~is in the median~~ are 0.01 - 0.07 fractional cloud coverage. The IRCCAM has an agreement of ±2 oktas (±0.25) in more than 90 % of cases and an agreement of ±1 okta (±0.125) in up to 77 % of the cases in comparison to other instruments. Thus, in only 10 % of the data, the IRCCAM typically overestimates the cloud fraction in comparison with the cloud fraction determined from the all-sky cameras sensitive in the visible region of

20   the spectrum. Differences in the cloud fraction estimates can be due to different thresholds for the camera systems (as discussed in Calbo et al. (2017)) as well as some other issues addressed throughout the current study.

In general, there is no ~~significant~~ considerable difference in the performance of the IRCCAM in the different seasons. Analysis of the median values of the residuals between the cloud fraction determined from the IRCCAM with the ones calculated from APCADA shows ~~almost~~ no difference between day and ~~nighttime. However, the spread of the data is larger during~~

25   ~~nighttimethan during daytime~~night time, even though the standard deviation of the residuals is clearly higher during nighttime. The ~~differentiation of cloud classes shows that low-level clouds are best detected with all camera systems, followed by mid-level clouds. Although an additional algorithm is applied to detect high-level clouds from the IRCCAM images, they are not yet detected in all cases due to their very low emissivity~~cloud fraction determination of the three cameras is independent of cloud classes, with the exception of thin cirrus clouds which are underestimated by the current IRCCAM algorithm by about

30   0.13 cloud fraction.

Overall, the IRCCAM is able to determine cloud fraction with a good agreement in comparison to all-sky cameras sensitive in the visible spectrum and with no ~~significant~~ considerable differences in its performance during different times of the day or different seasons. Thus, the IRCCAM is a stable system that can be used 24 hours per day with a high temporal resolution. In

comparison to other state of the art cloud detection instruments (e.g. ceilometer or Nubiscope) it has the advantage of ~~depicting~~ measuring the whole upper hemisphere at one specific moment. Its accuracy ranges from similar to rather better than that of the Nubiscope (Feister et al., 2010) as well as that of the human observers (Boers et al., 2010).

In this study we mainly showed one application of the IRCCAM, which is to retrieve fractional cloud coverage information

5   from the images. However, the known brightness temperature distribution of the sky and thus the known radiance can also be used for other applications ~~such as for example to determine~~ including the determination of other cloud parameters (cloud type, cloud level, cloud optical thickness) as well as ~~to retrieve~~ the retrieval of information about downward longwave radiation in general. Thus, after some improvements in the hardware (e.g. a heating or ventilation system to avoid a frozen mirror) and software (improvements of the cloud algorithm detecting ~~high-level clouds~~ low-emissivity clouds by e.g. pattern recognition)

10 the IRCCAM might be of interest for a number of further applications for example at meteorological stations or airports.

16

References

Ackerman, S. A., Holz, R. E., Frey, R., Eloranta, E. W., Maddux, B. C., and McGill, M.: Cloud Detection with MODIS. Part II: Validation, Journal of Atmospheric and Oceanic Technology, 25, 1073–1086, doi:10.1175/2007JTECHA1053.1, https://doi.org/10.1175/2007JTECHA1053.1, 2008.

5 Aebi, C., Gröbner, J., Kämpfer, N., and Vuilleumier, L.: Cloud radiative effect, cloud fraction and cloud type at two stations in Switzerland using hemispherical sky cameras, Atmospheric Measurement Techniques, 10, 4587–4600, doi:10.5194/amt-10-4587-2017, https://www.atmos-meas-tech.net/10/4587/2017/, 2017.

Baum B.A., P. S.: Introduction to MODIS Cloud Products, In Earth Science Satellite Remote Sensing., Springer, Berlin, Heidelberg, 2006.

Berger, L., Besnard, T., Genkova, I., Gillotay, D., Long, C., Zanghi, F., Deslondes, J. P., and Perdereau, G.: Image comparison from two cloud

10 cover sensor in infrared and visible spectral regions, in: 21st International Conference on Interactive Information Processing Systems (IIPS) for Meteorology, Oceanography, and Hydrology, 2005.

Berk, A., Anderson, G. P., Acharya, P. K., Bernstein, L. S., Muratov, L., Lee, J., Fox, M. J., Adler-Golden, S. M., Chetwynd, J. H., Hoke, M. L., Lockwood, R. B., Cooley, T. W., and Gardner, J. A.: MODTRAN5: a reformulated atmospheric band model with auxiliary species and practical multiple scattering options, Proc. SPIE, 5655, 88–95, doi:10.1117/12.578758, http://dx.doi.org/10.1117/12.578758, 2005.

15 Boers, R., de Haij, M. J., Wauben, W. M. F., Baltink, H. K., van Ulft, L. H., Savenije, M., and Long, C. N.: Optimized fractional cloudiness determination from five ground-based remote sensing techniques, Journal of Geophysical Research: Atmospheres, 115, doi:10.1029/2010JD014661, http://dx.doi.org/10.1029/2010JD014661, d24116, 2010.

Brede, B., Thies, B., Bendix, J., and Feister, U.: Spatiotemporal High-Resolution Cloud Mapping with a Ground-Based IR Scanner, Advances in Meteorology, 2017, doi:https://doi.org/10.1155/2017/6149831., 2017.

20 Brocard, E., Schneebeli, M., and Matzler, C.: Detection of Cirrus Clouds Using Infrared Radiometry, IEEE Transactions on Geoscience and Remote Sensing, 49, 595–602, doi:10.1109/TGRS.2010.2063033, 2011.

Calbo, J. and Sabburg, J.: Feature Extraction from Whole-Sky Ground-Based Images for Cloud-Type Recognition, Journal of Atmospheric and Oceanic Technology, 25, 3–14, doi:10.1175/2007JTECHA959.1, https://doi.org/10.1175/2007JTECHA959.1, 2008.

Calbo, J., Gonzalez, J.-A., and Pagas, D.: A Method for Sky-Condition Classification from Ground-Based Solar Radia-

25 tion Measurements, Journal of Applied Meteorology, 40, 2193–2199, doi:10.1175/1520-0450(2001)040<2193:AMFSCC>2.0.CO;2, https://doi.org/10.1175/1520-0450(2001)040<2193:AMFSCC>2.0.CO;2, 2001.

Calbo, J., Jordi, B., Gonzalez, J. A., Lidya, D., Valentina, K., Aaron, E.-A., and Arturo, S.-L.: Climatology and changes in cloud cover in the area of the Black, Caspian, and Aral seas (1991-2010): a comparison of surface observations with satellite and reanalysis products, International Journal of Climatology, 36, 1428–1443, doi:10.1002/joc.4435, https://rmets.onlinelibrary.wiley.com/doi/abs/10.1002/joc.4435,

30 2016.

Calbo, J., Long, C. N., Gonzalez, J.-A., Augustine, J., and McComiskey, A.: The thin border between cloud and aerosol: Sensitivity of several ground based observation techniques, Atmospheric Research, 196, 248 – 260, doi:https://doi.org/10.1016/j.atmosres.2017.06.010, http://www.sciencedirect.com/science/article/pii/S0169809517301047, 2017.

Campbell, J. R., Hlavka, D. L., Welton, E. J., Flynn, C. J., Turner, D. D., Spinhirne, J. D., III, V. S. S., and Hwang, I. H.: Full-Time,

35 Eye-Safe Cloud and Aerosol Lidar Observation at Atmospheric Radiation Measurement Program Sites: Instruments and Data Processing, Journal of Atmospheric and Oceanic Technology, 19, 431–442, doi:10.1175/1520-0426(2002)019<0431:FTESCA>2.0.CO;2, https://doi.org/10.1175/1520-0426(2002)019<0431:FTESCA>2.0.CO;2, 2002.

Cazorla, A., Olmo, F. J., and Alados-Arboledas, L.: Development of a sky imager for cloud cover assessment, J. Opt. Soc. Am. A, 25, 29–39, doi:10.1364/JOSAA.25.000029, http://josaa.osa.org/abstract.cfm?URI=josaa-25-1-29, 2008.

Chernokulsky, A. V., Esau, I., Bulygina, O. N., Davy, R., Mokhov, I. I., Outten, S., and Semenov, V. A.: Climatology and Interannual Variability of Cloudiness in the Atlantic Arctic from Surface Observations since the Late Nineteenth Century, Journal of Climate, 30, 2103–2120, doi:10.1175/JCLI-D-16-0329.1, https://doi.org/10.1175/JCLI-D-16-0329.1, 2017.

CIMO: Guide to Meteorological Instruments and Methods of Observation, World Meteorological Organization Bulletin, 8, 2014.

Da, C.: Preliminary assessment of the Advanced Himawari Imager (AHI) measurement onboard Himawari-8 geostationary satellite, Remote Sensing Letters, 6, 637–646, doi:10.1080/2150704X.2015.1066522, https://doi.org/10.1080/2150704X.2015.1066522, 2015.

Dürr, B. and Philipona, R.: Automatic cloud amount detection by surface longwave downward radiation measurements, J. Geophys. Res., 109, D05 201, doi:10.1029/2003JD004182, 2004.

Dybbroe, A., Karlsson, K.-G., and Thoss, A.: NWCSAF AVHRR Cloud Detection and Analysis Using Dynamic Thresholds and Radiative Transfer Modeling. Part I: Algorithm Description, Journal of Applied Meteorology, 44, 39–54, doi:10.1175/JAM-2188.1, https://doi.org/10.1175/JAM-2188.1, 2005.

Feister, U. and Shields, J.: Cloud and radiance measurements with the VIS/NIR Daylight Whole Sky Imager at Lindenberg (Germany), Meteorologische Zeitschrift, 14, 627–639, doi:10.1127/0941-2948/2005/0066, http://dx.doi.org/10.1127/0941-2948/2005/0066, 2005.

Feister, U., Möller, H., Sattler, T., Shields, J., Görsdorf, U., and Güldner, J.: Comparison of macroscopic cloud data from ground-based measurements using VIS/NIR and IR instruments at Lindenberg, Germany, Atmospheric Research, 96, 395 – 407, doi:https://doi.org/10.1016/j.atmosres.2010.01.012, http://www.sciencedirect.com/science/article/pii/S0169809510000232, 15th International Conference on Clouds and Precipitation, 2010.

Fontana, F., Lugrin, D., Seiz, G., Meier, M., and Foppa, N.: Intercomparison of satellite- and ground-based cloud fraction over Switzerland (2000–2012), Atmospheric Research, 128, 1 – 12, doi:https://doi.org/10.1016/j.atmosres.2013.01.013, http://www.sciencedirect.com/science/article/pii/S0169809513000525, 2013.

Gröbner, J.: Operation and investigation of a tilted bottom cavity for pyrgeometer characterizations, Appl. Opt., 47, 4441–4447, doi:10.1364/AO.47.004441, http://ao.osa.org/abstract.cfm?URI=ao-47-24-4441, 2008.

Heinle, A., Macke, A., and Srivastav, A.: Automatic cloud classification of whole sky images, Atmos. Meas. Tech., 3, 557–567, doi:10.5194/amt-3-557-2010, 2010.

Heymsfield, A. J., Krämer, M., Luebke, A., Brown, P., Cziczo, D. J., Franklin, C., Lawson, P., Lohmann, U., McFarquhar, G., Ulanowski, Z., and Tricht, K. V.: Cirrus Clouds, Meteorological Monographs, 58, 2.1–2.26, doi:10.1175/AMSMONOGRAPHS-D-16-0010.1, https://doi.org/10.1175/AMSMONOGRAPHS-D-16-0010.1, 2017.

Huertas-Tato, J., J., R.-B. F., C., A.-B., R., A.-M., I., G.-L., and D., P.-V.: Automatic Cloud-Type Classification Based On the Combined Use of a Sky Camera and a Ceilometer, Journal of Geophysical Research: Atmospheres, 122, 11,045–11,061, doi:10.1002/2017JD027131, https://agupubs.onlinelibrary.wiley.com/doi/abs/10.1002/2017JD027131, 2017.

Illingworth, A. J., Hogan, R. J., O'Connor, E., Bouniol, D., Brooks, M. E., Delanoé, J., Donovan, D. P., Eastment, J. D., Gaussiat, N., Goddard, J. W. F., Haeffelin, M., Baltink, H. K., Krasnov, O. A., Pelon, J., Piriou, J.-M., Protat, A., Russchenberg, H. W. J., Seifert, A., Tompkins, A. M., van Zadelhoff, G.-J., Vinit, F., Willén, U., Wilson, D. R., and Wrench, C. L.: Cloudnet: Continuous Evaluation of Cloud Profiles in Seven Operational Models Using Ground-Based Observations, Bulletin of the American Meteorological Society, 88, 883–898, doi:10.1175/BAMS-88-6-883, https://doi.org/10.1175/BAMS-88-6-883, 2007.

Kato, S., Mace, G. G., Clothiaux, E. E., Liljegren, J. C., and Austin, R. T.: Doppler Cloud Radar Derived Drop Size Distributions in Liquid Water Stratus Clouds, Journal of the Atmospheric Sciences, 58, 2895–2911, doi:10.1175/1520-0469(2001)058<2895:DCRDDS>2.0.CO;2, https://doi.org/10.1175/1520-0469(2001)058<2895:DCRDDS>2.0.CO;2, 2001.

5 Kazantzidis, A., Tzoumanikas, P., Bais, A. F., Fotopoulos, S., and Economou, G.: Cloud detection and classification with the use of whole-sky ground-based images, Atmos. Res., 113, 80–88, doi:10.1016/j.atmosres.2012.05.005, 2012.

Klebe, D. I., Blatherwick, R. D., and Morris, V. R.: Ground-based all-sky mid-infrared and visible imagery for purposes of characterizing cloud properties, Atmospheric Measurement Techniques, 7, 637–645, doi:10.5194/amt-7-637-2014, https://www.atmos-meas-tech.net/7/637/2014/, 2014.

10 Kotarba, A. Z.: Inconsistency of surface-based (SYNOP) and satellite-based (MODIS) cloud amount estimations due to the interpretation of cloud detection results, International Journal of Climatology, 37, 4092–4104, doi:10.1002/joc.5011, https://rmets.onlinelibrary.wiley.com/doi/abs/10.1002/joc.5011, 2017.

Kuhn, P., Bijan, N., Stefan, W., Christoph, P., Nora, K., Thomas, S., Zeyad, Y., Lourdes, R., Luis, Z., Angela, M., Laurent, V., Detlev, H., Philippe, B., and Robert, P.-P.: Validation of an all-sky imager-based nowcasting system for industrial PV plants, Progress in Photovoltaics:
15 Research and Applications, doi:10.1002/pip.2968, https://onlinelibrary.wiley.com/doi/abs/10.1002/pip.2968, 2017.

Liu, L., jin Sun, X., chang Gao, T., and jun Zhao, S.: Comparison of Cloud Properties from Ground-Based Infrared Cloud Measurement and Visual Observations, Journal of Atmospheric and Oceanic Technology, 30, 1171–1179, doi:10.1175/JTECH-D-12-00157.1, https://doi.org/10.1175/JTECH-D-12-00157.1, 2013.

Liu, L., jin Sun, X., chuan Liu, X., chang Gao, T., and jun Zhao, S.: Comparison of Cloud Base Height Derived from a Ground-
20 Based Infrared Cloud Measurement and Two CeilometersAdvances in Meteorology, vol. 2015, Article ID 853861, 8 pages, 2015. doi:10.1155/2015/853861, Advances in Meteorology, 2015, doi:doi:10.1155/2015/853861, 2015.

Long, C. N., Sabburg, J. M., Calbo, J., and Pages, D.: Retrieving cloud characteristics from ground-based daytime color all-sky images, J. Atmos. Oceanic Technol., 23, 633–652, doi:10.1175/JTECH1875.1, 2006.

Martucci, G., Milroy, C., and O'Dowd, C. D.: Detection of Cloud-Base Height Using Jenoptik CHM15K and Vaisala
25 CL31 Ceilometers, Journal of Atmospheric and Oceanic Technology, 27, 305–318, doi:10.1175/2009JTECHA1326.1, https://doi.org/10.1175/2009JTECHA1326.1, 2010.

Mateos, D., Anton, M., Valenzuela, A., Cazorla, A., Olmo, F., and Alados-Arboledas, L.: Efficiency of clouds on shortwave radiation using experimental data, Appl. Energy, 113, 1216 – 1219, doi:http://dx.doi.org/10.1016/j.apenergy.2013.08.060, http://www.sciencedirect.com/science/article/pii/S0306261913007046, 2014.

30 Mateos Villàn, D., de Miguel Castrillo, A., and Bilbao Santos, J.: Empirical models of UV total radiation and cloud effect study, International Journal of Climatology, 30, 1407–1415, doi:10.1002/joc.1983, http://dx.doi.org/10.1002/joc.1983, 2010.

Morland, J., Deuber, B., Feist, D. G., Martin, L., Nyeki, S., Kämpfer, N., Mätzler, C., Jeannet, P., and Vuilleumier, L.: The STARTWAVE atmospheric water database, Atmos. Chem. Phys., 6, 2039–2056, doi:10.5194/acp-6-2039-2006, http://www.atmos-chem-phys.net/6/2039/2006/, 2006.

35 Parida, B., Iniyan, S., and Goic, R.: A review of solar photovoltaic technologies, Renewable and Sustainable Energy Reviews, 15, 1625 – 1636, doi:https://doi.org/10.1016/j.rser.2010.11.032, http://www.sciencedirect.com/science/article/pii/S1364032110004016, 2011.

Redman, B. J., Shaw, J. A., Nugent, P. W., Clark, R. T., and Piazzolla, S.: Reflective all-sky thermal infrared cloud imager, Opt. Express, 26, 11 276–11 283, doi:10.1364/OE.26.011276, http://www.opticsexpress.org/abstract.cfm?URI=oe-26-9-11276, 2018.

Ricciardelli, E., Romano, F., and Cuomo, V.: A Technique for Classifying Uncertain MOD35/MYD35 Pixels Through Meteosat Second Generation-Spinning Enhanced Visible and Infrared Imager Observations, IEEE Transactions on Geoscience and Remote Sensing, 48, 2137–2149, doi:10.1109/TGRS.2009.2035367, 2010.

Shaw, J. A., Nugent, P. W., Pust, N. J., Thurairajah, B., and Mizutani, K.: Radiometric cloud imaging with an uncooled microbolometer thermal infrared camera, Opt. Express, 13, 5807–5817, doi:10.1364/OPEX.13.005807, http://www.opticsexpress.org/abstract.cfm?URI=oe-13-15-5807, 2005.

Shields, J. E., Karr, M. E., Johnson, R. W., and Burden, A. R.: Day/night whole sky imagers for 24-h cloud and sky assessment: history and overview, Appl. Opt., 52, 1605–1616, doi:10.1364/AO.52.001605, http://ao.osa.org/abstract.cfm?URI=ao-52-8-1605, 2013.

Smith, C. J., Bright, J. M., and Crook, R.: Cloud cover effect of clear-sky index distributions and differences between human and automatic cloud observations, Solar Energy, 144, 10 – 21, doi:https://doi.org/10.1016/j.solener.2016.12.055, http://www.sciencedirect.com/science/article/pii/S0038092X16306624, 2017.

Smith, S. and Toumi, R.: Measuring cloud cover and brightness temperature with a ground-based thermal infrared camera, J. Appl. Meteorol. Climatol., 47, 683–693, doi:10.1175/2007JAMC1615.1, 2008.

Tapakis, R. and Charalambides, A. G.: Equipment and methodologies for cloud detection and classification: A review, Sol. Energy, 95, 392–430, doi:10.1016/j.solener.2012.11.015, 2013.

Thurairajah, B. and Shaw, J. A.: Cloud statistics measured with the infrared cloud imager (ICI), IEEE Transactions on Geoscience and Remote Sensing, 43, 2000–2007, doi:10.1109/TGRS.2005.853716, 2005.

Tzoumanikas, P., Nikitidou, E., Bais, A., and Kazantzidis, A.: The effect of clouds on surface solar irradiance, based on data from an all-sky imaging system, Renew. Energy, 95, 314 – 322, doi:http://dx.doi.org/10.1016/j.renene.2016.04.026, http://www.sciencedirect.com/science/article/pii/S0960148116303305, 2016.

Wacker, S., Gröbner, J., Zysset, C., Diener, L., Tzoumanikas, P., Kazantzidis, A., Vuilleumier, L., Stoeckli, R., Nyeki, S., and Kämpfer, N.: Cloud observations in Switzerland using hemispherical sky cameras, J. Geophys. Res., 120, 695–707, doi:10.1002/2014JD022643, 2015.

Wauben, W.: Evaluation of the Nubiscope, Technisch rapport / Koninklijk Nederlands Meteorologisch Instituut, 291, 37., 2006.

Werkmeister, A., Lockhoff, M., Schrempf, M., Tohsing, K., Liley, B., and Seckmeyer, G.: Comparing satellite- to ground-based automated and manual cloud coverage observations - a case study, Atmos. Meas. Tech., 8, 2001–2015, doi:10.5194/amt-8-2001-2015, 2015.

WMO: Recommended methods for evaluating cloud and related parameters World Weather Research PRogramm (WWRP)/Working Group on Numerical Experimentation (WGNE) Joint Working Group on Forecase Verification Research (JWGFVR),, Document WWRP 2012-1, March, 2012.

Zhao, C., Wang, Y., Wang, Q., Li, Z., Wang, Z., and Liu, D.: A new cloud and aerosol layer detection method based on micropulse lidar measurements, Journal of Geophysical Research: Atmospheres, 119, 6788–6802, doi:10.1002/2014JD021760, http://dx.doi.org/10.1002/2014JD021760, 2014JD021760, 2014.

Figure 1. The Infrared Cloud Camera (IRCCAM) in the measurement enclosure of PMOD/WRC in Davos, Switzerland.
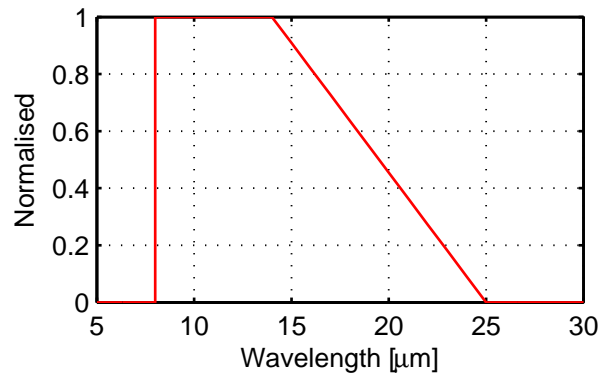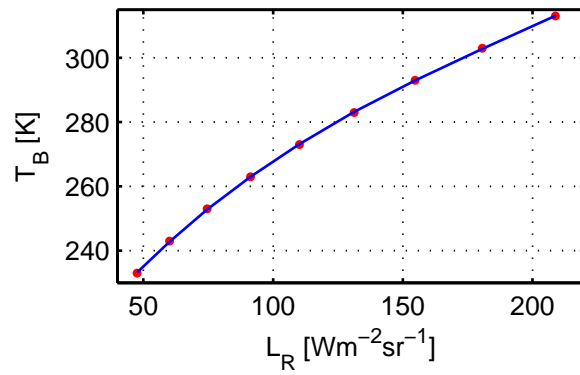
**Figure 2.** ~~Brightness Temperature T_B versus integrated radiance L_{8-14} for different radiance values (red dots), and the corresponding third order polynomial fitting~~ Response function ~~(blue line)~~ R_λ of the camera of the IRCCAM instrument.

Figure 3. Brightness Temperature T_B versus integrated radiance L_R for different radiance values (red dots), and the corresponding third order polynomial fitting function (blue line).
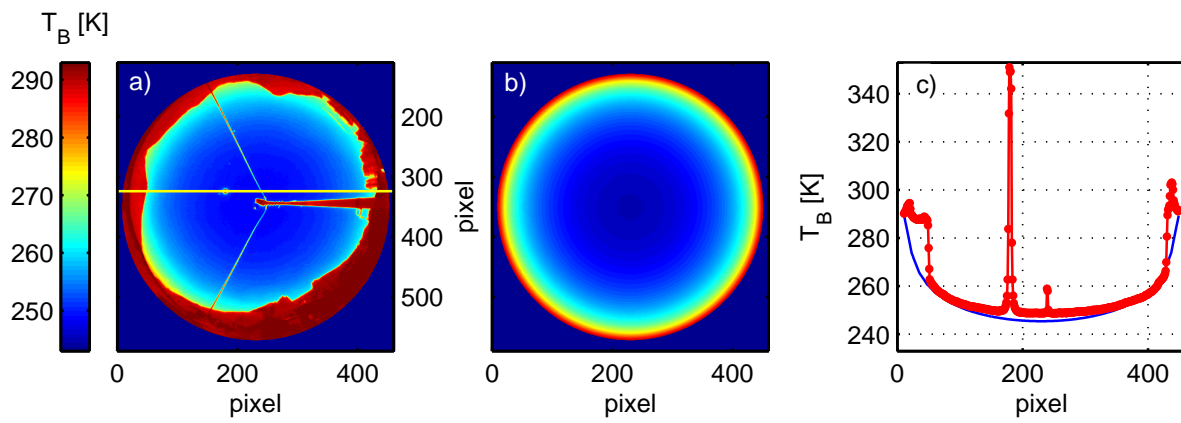
Figure 4. (a) Measured brightness temperature on the cloud-free day June 18, 2017 10:49 UTC (SZA=~~23~~24 °), (b) the corresponding modelled brightness temperature and (c) the measured (red) and modelled (blue) profile of the sky brightness temperature along one azimuth position (shown as a yellow line in (a)).
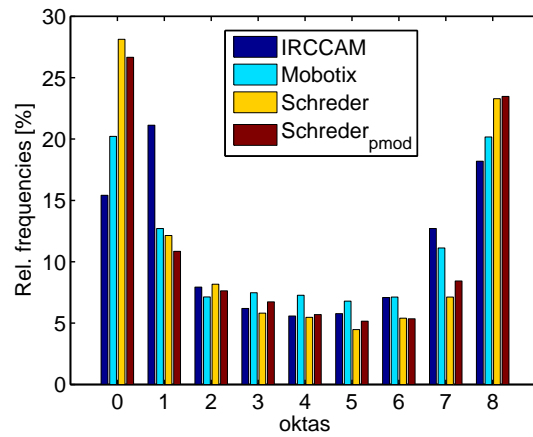
Figure 5. Relative frequencies of the determined cloud coverage of the study instruments for selected bins of cloud coverages at Davos. Zero okta: 0 - 0.0500.0500; 1 okta: 0.0500.0500 - 0.1250.1875; 2 oktas: 0.1250.1875 - 0.2500.3125; 3 oktas: 0.2500.3125 - 0.3750.4375; 4 oktas: 0.3750.4375 - 0.5000.5625; 5 oktas: 0.5000.5625 - 0.6250.6875; 6 oktas: 0.6250.6875 - 0.7500.8125; 7 oktas: 0.7500.8125 - 0.8750.9500; 8 oktas: 0.8750.9500 - 1;
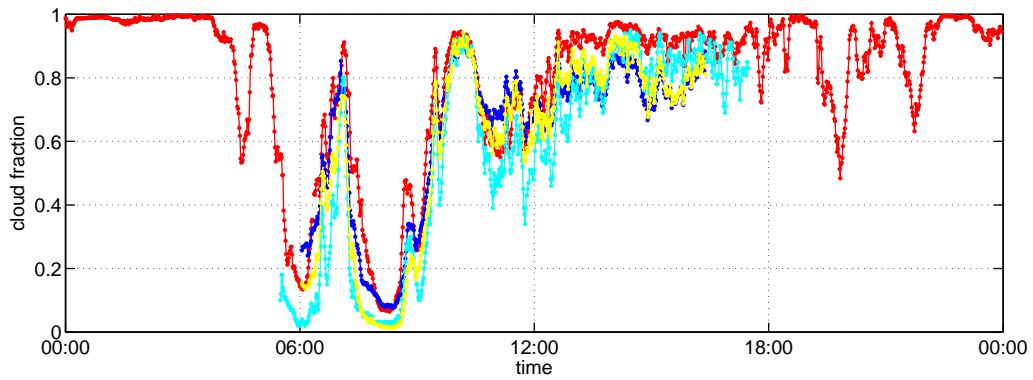
Figure 6. Cloud fraction determined by the study instruments and algorithms (red: IRCCAM, blue: Mobotix, cyan: Schreder, yellow: Schreder_pmod) on April 4, 2016.
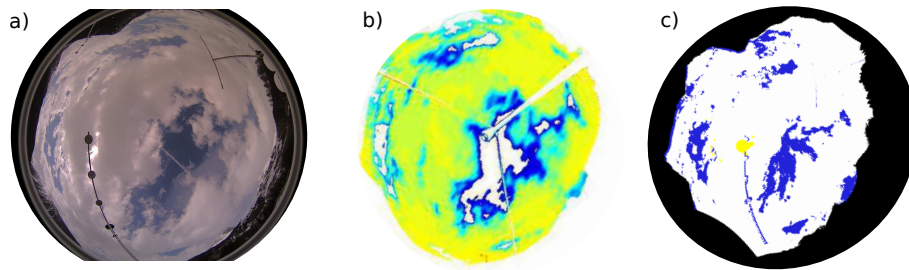
Figure 7. The cloud situation on April 4, 2016 10 UTC on an image from Mobotix (a) and the cloud fraction determined from (b) IRCCAM (temperature range from 244 K (blue) to 274 K (yellow)) and (c) Mobotix (white: clouds, blue: cloud-free, yellow: area around sun).
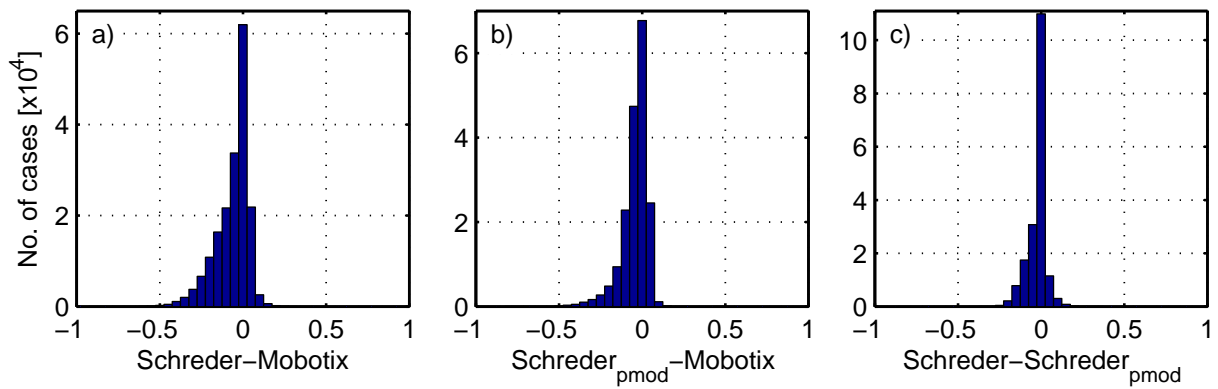
Figure 8. Residuals of the comparison of cloud fraction retrieved from the visible cameras and algorithms used in the study.
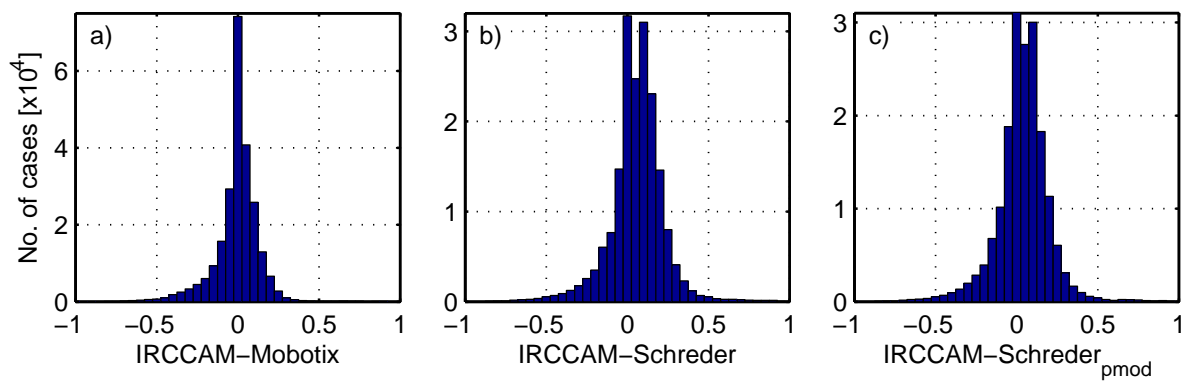
Figure 9. Residuals of the comparison of cloud fraction retrieved from the IRCCAM versus cloud fraction retrieved from the visible cameras.
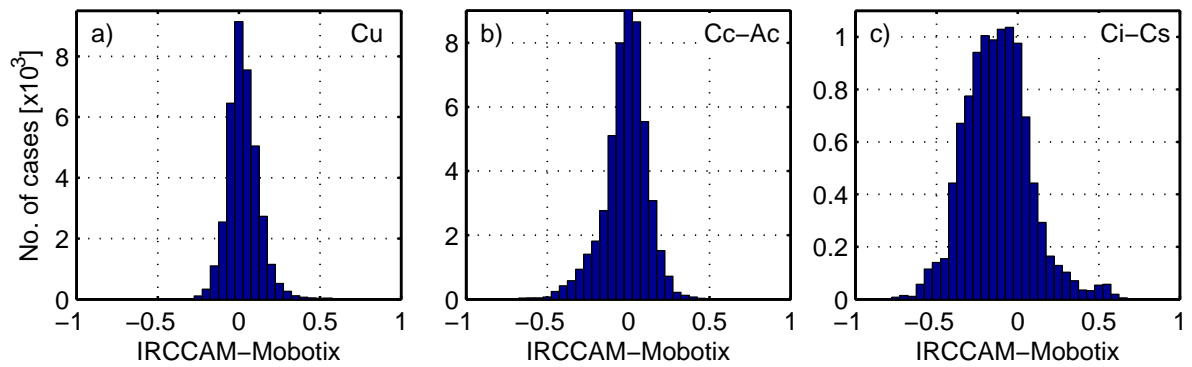
Figure 10. Residuals of the comparison of cloud fraction determined from IRCCAM images versus cloud fraction determined from Mobotix images for the following cloud classes: Cu: Cumulus, Cc-Ac: Cirrocumulus-Altocumulus, Ci-Cs: Cirrus-Cirrostratus

Table 1. Median and 5th and 95th percentiles of the differences in calculated cloud fractions from the visible all-sky cameras and APCADA. The numbers are in the range [-1;1].

	Cloud fraction		
	median	5th	95th
Schreder - Mobotix	-0.03	-0.26	0.05
Schreder$_{pmod}$ - Mobotix	-0.02	-0.19	0.04
Schreder - Schreder$_{pmod}$	0.00	-0.13	0.04
APCADA - Mobotix	-0.04	-0.43	0.17
APCADA - Schreder	-0.01	-0.38	0.30
APCADA - Schreder$_{pmod}$	-0.01	-0.38	0.26

Table 2. Median and 5th and 95th percentiles of the differences in calculated cloud fractions between IRCCAM and the visible all-sky cameras.

	Cloud fraction		
	median	5th	95th
IRCCAM - Mobotix	0.01	-0.26	0.18
IRCCAM - Schreder	0.07	-0.22	0.29
IRCCAM - Schreder$_{pmod}$	0.04	-0.23	0.26

~~Residuals of the comparison of cloud fraction retrieved from the IRCCAM versus cloud fraction retrieved from the visible cameras.~~

Table 3. ~~Residuals~~ Percentage of ~~the comparison of~~ fractional cloud ~~fraction determined from IRCCAM images versus cloud fraction determined from Mobotix images for~~ coverage data which agree within ± 1 okta (all values above the ~~following cloud classes: Cu: Cumulus, Cc-Ac: Cirrocumulus-Altocumulus, Ci-Cs: Cirrus-Cirrostratus~~ grey cells) and ± 2 oktas (all values below the grey cells) when comparing two algorithms each.

	IRCCAM	Mobotix	Schreder	Schreder$_{pmod}$	APCADA
IRCCAM	-	77%	59%	66%	62%
Mobotix	93%	-	77%	89%	67%
Schreder	88%	94%	-	94%	71%
Schreder$_{pmod}$	90%	97%	100%	-	70%
APCADA	80%	83%	86%	85%	-

Table 4. Median and 5th and 95th percentiles of the differences in calculated cloud fractions from IRCCAM and Mobotix images for selected cloud classes (stratocumulus (Sc), cumulus (Cu), stratus-altostratus (St-As), cumulonimbus-nimbostratus (Cb-Ns), cirrocumulus-altocumulus (Cc-Ac), cirrus-cirrostratus (Ci-Cs) and cloud-free (Cf).

	Cloud fraction		
	median	5th	95th
Sc	0.01	-0.24	0.21
Cu	0.02	-0.12	0.19
St-As	0.00	-0.38	0.11
Cb-Ns	-0.01	-0.22	0.08
Cc-Ac	0.00	-0.27	0.18
Ci-Cs	-0.13	-0.42	0.21
Cf	0.03	-0.03	0.18

Table 5. Median and 5th and 95th percentiles of the differences in calculated cloud fractions from IRCCAM versus APCADA: overall; only daytime and only nighttime.

	Cloud fraction		
	median	5th	95th
IRCCAM - APCADA	0.05	-0.31	0.54
IRCCAM - APCADA day	0.06	-0.18	0.35
IRCCAM - APCADA night	0.04	-0.40	0.65

Table 6. ~~Percentage of fractional cloud coverage data which agree within ±1 okta (all~~ Identical to Table 3, but left-hand are the values ~~above~~ for the ~~grey cells~~summer months (June, July, August) and ~~±2 oktas (all~~ right-hand the values ~~below~~ for the ~~grey cells~~winter months (December, January, February)~~comparing two algorithms each~~.

	IRCCAM
IRCCAM	- ~~77% 59% 66% 62% Mobotix 93% - 77% 89% 67% Schreder 88% 94% - 94%~~ 71% ~~Schreder_{pmod} 90% 97% 100% - 70%~~
Mobotix	91% | 94%
Schreder	89% | 84%
Schreder$_{pmod}$	89% | 86%
APCADA	87% | 65%